

Vibronic Effects on the Quantum Tunnelling of Magnetisation in Single-Molecule Magnets

Andrea Mattioni,^{1,*} Jakob K. Staab,¹ William J. A. Blackmore,¹ Daniel Reta,^{1,2} Jake Iles-Smith,^{3,4} Ahsan Nazir,³ and Nicholas F. Chilton^{1,†}

¹*Department of Chemistry, School of Natural Sciences,
The University of Manchester, Oxford Road, Manchester, M13 9PL, UK*

²*Faculty of Chemistry, UPV/EHU & Donostia International Physics Center DIPC,
Ikerbasque, Basque Foundation for Science, Bilbao, Spain*

³*Department of Physics and Astronomy, School of Natural Sciences,
The University of Manchester, Oxford Road, Manchester M13 9PL, UK*

⁴*Department of Electrical and Electronic Engineering, School of Engineering,
The University of Manchester, Sackville Street Building, Manchester M1 3BB, UK*

Single-molecule magnets are among the most promising platforms for achieving molecular-scale data storage and processing. Their magnetisation dynamics are determined by the interplay between electronic and vibrational degrees of freedom, which can couple coherently, leading to complex vibronic dynamics. Building on an *ab initio* description of the electronic and vibrational Hamiltonians, we formulate a non-perturbative vibronic model of the low-energy magnetic degrees of freedom in a single-molecule magnet, which we benchmark against field-dependent magnetisation measurements. Describing the low-temperature magnetism of the complex in terms of magnetic polarons, we are able to quantify the vibronic contribution to the quantum tunnelling of the magnetisation. Despite collectively enhancing magnetic relaxation, we observe that specific vibrations suppress quantum tunnelling by enhancing the magnetic axiality of the complex. Finally, we discuss how this observation might impact the current paradigm to chemical design of new high-performance single-molecule magnets, promoting vibrations to an active role rather than just regarding them as sources of noise and decoherence.

I. INTRODUCTION

Single-molecule magnets (SMMs) hold the potential for realising high-density data storage and quantum information processing [1–4]. These molecules exhibit a doubly-degenerate ground state, comprising two states supporting a large magnetic moment with opposite orientation, which represents an ideal platform for storing digital data. Slow reorientation of this magnetic moment results in magnetic hysteresis at the single-molecule level at sufficiently low temperatures [5]. The main obstacle to extending this behaviour to room temperature is the coupling of the magnetic degrees of freedom to molecular and lattice vibrations, often referred to as spin-phonon coupling. Thermal excitation of the molecular vibrations cause transitions between different magnetic states, ultimately leading to a complete loss of magnetisation. Advances in design, synthesis and characterisation of SMMs have shed light on the microscopic mechanisms underlying their desirable magnetic properties, extending this behaviour to increasingly higher temperatures [6–8].

The mechanism responsible for magnetic relaxation in SMMs strongly depends on temperature. At higher temperatures, relaxation is driven by one (Orbach) and two (Raman) phonon transitions between magnetic sublevels [9]. When temperatures approach absolute zero, all vibrations are predominantly found in their ground state. Thus, both Orbach and Raman transitions become negligible and the dominant mechanism is quantum tunnelling of the magnetisation

(QTM) between the two degenerate ground states [10, 11]. This process relies on the presence of a coherent coupling mixing the two otherwise degenerate ground states, opening a tunnelling gap, and allowing population to redistribute between them, thus leading to facile magnetic reorientation.

While the role of vibrations in high-temperature magnetic relaxation is well understood in terms of weak-coupling rate equations for the electronic populations [12–15], the connection between QTM and spin-phonon coupling is still unclear. Some analyses have looked at the influence of vibrations on QTM in integer-spin SMMs, where a model spin system was used to show that spin-phonon coupling could open a tunnelling gap [16, 17]. However, QTM remains more elusive to grasp in half-integer spin complexes, such as monometallic Dy(III) SMMs, since it is observed experimentally despite being forbidden by Kramers theorem [18]. In this case, a magnetic field is needed to break the time-reversal symmetry of the molecular Hamiltonian and lift the degeneracy of the ground doublet. This magnetic field can be provided by hyperfine interaction with nuclear spins or by dipolar coupling to other SMMs; both these effects have been shown to affect tunnelling behaviour [19–25]. Once the tunnelling gap is opened by a magnetic field, molecular vibrations can in principle affect its magnitude in a nontrivial way. In a recent work, Ortu *et al.* analysed the magnetic hysteresis of a series of Dy(III) SMMs, suggesting that QTM efficiency correlates with molecular flexibility [22]. In another work, hyperfine coupling was proposed to assist QTM by facilitating the interaction between molecular vibrations and spin sublevels [26]. However, a clear and unambiguous demonstration of the influence of the spin-phonon coupling on QTM beyond toy-model approaches is still lacking to this date.

In this work we present a theoretical analysis of the effect of

* andrea.mattioni@manchester.ac.uk

† nicholas.chilton@manchester.ac.uk

molecular vibrations on the tunnelling dynamics in a Dy(III) SMM. In contrast to previous treatments, our approach is based on a fully *ab initio* description of the SMM vibrational environment and accounts for the spin-phonon coupling in a non-perturbative way, overcoming the standard weak-coupling master equation approach commonly used to determine the high-temperature magnetisation dynamics. After deriving an effective low-energy model for the relevant vibronic degrees of freedom based on a polaron approach [27], we demonstrate that vibrations can either enhance or reduce the quantum tunnelling gap, depending on the orientation of the magnetic field relative to the main anisotropy axis of the SMM. Moreover, we validate our vibronic model against frozen solution, field-dependent magnetisation measurements and show that vibronic effects on QTM survive the orientational averaging imposed by amorphous samples, leading, on average, to a significant enhancement of the tunnelling probability. Lastly, we argue that not all vibrations lead to faster QTM; depending on how strongly vibrations impact the axiality of the lowest energy magnetic doublet, we show that they can play a benign role by suppressing tunnelling, and discuss first steps in that direction.

II. MODEL

The compound investigated in this work is $[\text{Dy}(\text{Cp}^{\text{ttt}})_2]^+$, shown in Fig. 1a [6]. The complex consists of a dysprosium ion Dy(III) enclosed between two negatively charged cyclopentadienyl rings with *tert*-butyl groups at positions 1, 2 and 4 (Cp^{ttt}). The crystal field generated by the axial ligands makes the states with larger angular momentum energetically favourable, resulting in the energy level diagram sketched in Fig. 1b. The energy barrier separating the two degenerate ground states results in magnetic hysteresis, which was observed up to $T = 60$ K [6]. Magnetic hysteresis is hindered by QTM, which leads to a characteristic sudden drop of the magnetisation at zero magnetic field.

To single out the contribution of molecular vibrations, we focus on a magnetically diluted sample in a frozen solution of dichloromethane (DCM). Thus, our computational model consists of a solvated $[\text{Dy}(\text{Cp}^{\text{ttt}})_2]^+$ cation (see Section S1 for details; Fig. 1a), which provides a realistic description of the low-frequency vibrational environment, comprised of pseudo-acoustic vibrational modes (Fig. 1c). These constitute the basis to consider further contributions of dipolar and hyperfine interactions to QTM (Fig. 1b).

Once the equilibrium geometry and vibrational modes of the solvated SMM (which are in general combinations of molecular and solvent vibrations) are obtained at the density-functional level of theory (see Section S1), we proceed to determine the equilibrium electronic structure via complete active space self-consistent field spin-orbit (CASSCF-SO) calculations. The electronic structure is projected onto an effective crystal-field Hamiltonian, parametrised in terms of crystal field parameters. The spin-phonon couplings are obtained from a single CASSCF calculation, by computing the analytic derivatives of the molecular Hamiltonian with respect to the

nuclear coordinates [14] (see Section S1 for more details).

The lowest-energy angular momentum multiplet of $[\text{Dy}(\text{Cp}^{\text{ttt}})_2]^+$ ($J = 15/2$) can thus be described by the *ab initio* vibronic Hamiltonian

$$\hat{H} = \sum_m E_m |m\rangle\langle m| + \sum_j \hat{V}_j \otimes (\hat{b}_j + \hat{b}_j^\dagger) + \sum_j \omega_j \hat{b}_j^\dagger \hat{b}_j, \quad (1)$$

where E_m denotes the energy associated with the electronic state $|m\rangle$ and \hat{V}_j represent the spin-phonon coupling operators. The harmonic vibrational modes of the DCM-solvated $[\text{Dy}(\text{Cp}^{\text{ttt}})_2]^+$ are described in terms of their bosonic annihilation (creation) operators \hat{b}_j (\hat{b}_j^\dagger) and frequencies ω_j .

In the absence of magnetic fields, the Hamiltonian (1) is symmetric under time reversal. This symmetry results in a two-fold degeneracy of the energy levels E_m , whose corresponding eigenstates $|m\rangle$ and $|\bar{m}\rangle$ form a time-reversal conjugate Kramers doublet. The degeneracy is lifted by introducing a magnetic field \mathbf{B} , which couples to the electronic degrees of freedom via the Zeeman interaction $\hat{H}_{\text{Zee}} = \mu_B g_J \mathbf{B} \cdot \hat{\mathbf{J}}$, where g_J is the Landé g -factor and $\hat{\mathbf{J}}$ is the total angular momentum operator. To linear order in the magnetic field, each Kramers doublet splits into two energy levels $E_m \pm \Delta_m/2$ corresponding to the states

$$|m_+\rangle = \cos \frac{\theta_m}{2} |m\rangle + e^{i\phi_m} \sin \frac{\theta_m}{2} |\bar{m}\rangle \quad (2)$$

$$|m_-\rangle = -\sin \frac{\theta_m}{2} |m\rangle + e^{i\phi_m} \cos \frac{\theta_m}{2} |\bar{m}\rangle \quad (3)$$

where the energy splitting Δ_m and the mixing angles θ_m and ϕ_m are determined by the matrix elements of the Zeeman Hamiltonian on the subspace $\{|m\rangle, |\bar{m}\rangle\}$. In addition to the intra-doublet mixing described by Eqs. (2) and (3), the Zeeman interaction also mixes Kramers doublets at different energies. The ground doublet acquires contributions from higher-lying states

$$|1'_\pm\rangle = |1_\pm\rangle + \sum_{m \neq 1, \bar{1}} |m\rangle \frac{\langle m | \hat{H}_{\text{Zee}} | 1_\pm \rangle}{E_1 - E_m} + \mathcal{O}(B^2). \quad (4)$$

These states no longer form a time-reversal conjugate doublet, meaning that the spin-phonon coupling can now contribute to transitions between them.

Since QTM is typically observed at much lower temperatures than the energy gap between the lowest and first excited doublets (which here is ~ 660 K [6]), we focus on the perturbed ground doublet $|1'_\pm\rangle$. Within this subspace, the Hamiltonian $\hat{H} + \hat{H}_{\text{Zee}}$ takes the form

$$\begin{aligned} \hat{H}_{\text{eff}} = & E_1 + \frac{\Delta_1}{2} \sigma'_z + \sum_j \omega_j \hat{b}_j^\dagger \hat{b}_j \\ & + \sum_j \left(\langle 1 | \hat{V}_j | 1 \rangle - w_j^z \sigma'_z \right) \left(\hat{b}_j + \hat{b}_j^\dagger \right) \\ & - \sum_j \left(w_j^x \sigma'_x + w_j^y \sigma'_y \right) \left(\hat{b}_j + \hat{b}_j^\dagger \right). \end{aligned} \quad (5)$$

This Hamiltonian describes the interaction between vibrational modes and an effective spin one-half represented by the Pauli matrices $\sigma' = (\sigma'_x, \sigma'_y, \sigma'_z)$,

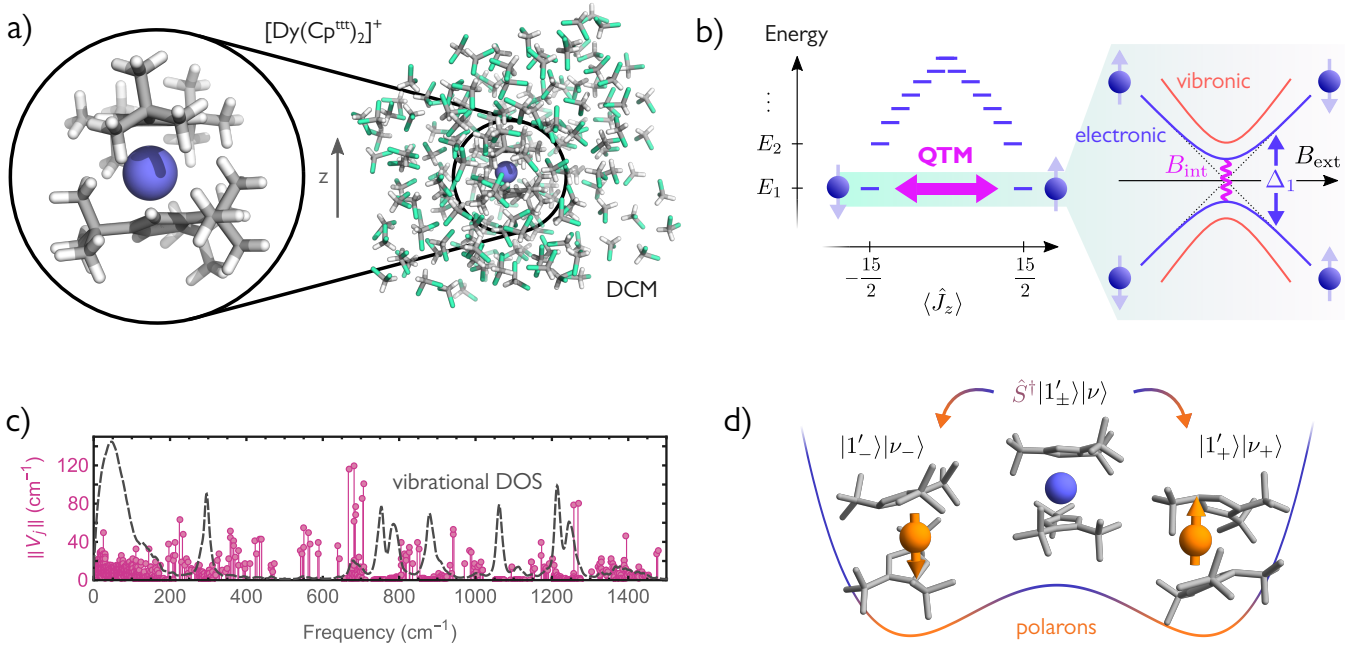


FIG. 1. **Quantum tunnelling in single-molecule magnets.** (a) Molecular structure of a Dy(III) single-molecule magnet surrounded by a dichloromethane bath. (b) Equilibrium energy level diagram of the lowest-energy angular momentum multiplet with $J = 15/2$. The second-lowest doublet at E_2 is 524 cm^{-1} higher than the ground doublet at E_1 , while the highest doublet is 1523 cm^{-1} above E_1 . Dipolar and hyperfine magnetic fields (B_{int}) can lift the degeneracy of the doublets and cause quantum tunnelling, which results in avoided crossings when sweeping an external magnetic field B_{ext} . Molecular vibrations can influence the magnitude of the avoided crossing. (c) Spin-phonon coupling for the solvated complex shown above, as a function of the vibrational frequency (vibrations with $\omega_j > 1500 \text{ cm}^{-1}$ not shown), calculated as the Frobenius norm of the operator \hat{V}_j . The grey dashed line represents the vibrational density of states, obtained by assigning to each molecular vibration a (anti-symmetrised) Lorentzian lineshape with full width at half-maximum 10 cm^{-1} (corresponding to a typical timescale of $\sim 1 \text{ ps}$). (d) Idea behind the polaron transformation of Eq. (6). Each spin state $|1'_{\pm}\rangle$ is accompanied by a vibrational distortion (greatly exaggerated for visualisation), thus forming a magnetic polaron. Vibrational states $|\nu\rangle$ are now described in terms of harmonic displacements around the deformed structure, which depends on the state of the spin. Polarons provide an accurate physical picture when the spin-phonon coupling is strong and mostly modulates the energy of different spin states but not the coupling between them.

where $\sigma'_z = |1'_+\rangle\langle 1'_+| - |1'_-\rangle\langle 1'_-|$. The vector $\mathbf{w}_j = (\Re\langle 1_-|\hat{W}_j|1_+\rangle, \Im\langle 1_-|\hat{W}_j|1_+\rangle, \langle 1_+|\hat{W}_j|1_+\rangle)$ is defined in terms of the operator $\hat{W}_j = \sum_{m \neq 1, \bar{1}} \hat{V}_j|m\rangle\langle m| \hat{H}_{\text{Zee}}/(E_m - E_1) + \text{h.c.}$, describing the effect of the Zeeman interaction on the spin-phonon coupling. Due to the strong magnetic axiality of the complex considered here, the longitudinal component of the spin-phonon coupling w_j^z dominates over the transverse part w_j^x, w_j^y (see Section S3). In this case, we can get a better physical picture of the system by transforming the Hamiltonian (5) to the polaron frame defined by the unitary operator

$$\hat{S} = \exp \left[\sum_{s=\pm} |1'_s\rangle\langle 1'_s| \sum_j \xi_j^s (\hat{b}_j^\dagger - \hat{b}_j) \right], \quad (6)$$

which mixes electronic and vibrational degrees of freedom by displacing the mode operators by $\xi_j^\pm = (\langle 1|\hat{V}_j|1\rangle \mp w_j^z)/\omega_j$ depending on the state of the effective spin one-half [27]. The idea behind this transformation is to allow nuclei to relax around a new equilibrium geometry, which may be different for every spin state. This lowers the energy of the system and provides a good description of the vibronic eigenstates

when the spin-phonon coupling is approximately diagonal in the spin basis (Fig. 1d). In the polaron frame, the longitudinal spin-phonon coupling is fully absorbed into the purely electronic part of the Hamiltonian, while the transverse components can be approximated by their thermal average over vibrations, neglecting their vanishingly small quantum fluctuations (see Section S2). After transforming back to the original frame, we are left with an effective spin one-half Hamiltonian with no residual spin-phonon coupling $H_{\text{eff}} \approx \hat{H}_{\text{eff}}^{(\text{pol})} + \sum_j \omega_j \hat{b}_j^\dagger \hat{b}_j$, where

$$\hat{H}_{\text{eff}}^{(\text{pol})} = E_1 + \frac{\Delta_1}{2} \sigma''_z + 2 \sum_j \frac{\langle 1|\hat{V}_j|1\rangle}{\omega_j} \mathbf{w}_j \cdot \sigma''. \quad (7)$$

The set of Pauli matrices $\sigma'' = \hat{S}^\dagger (\sigma' \otimes \mathbb{1}_{\text{vib}}) \hat{S}$ describe the two-level system formed by the magnetic polarons of the form $\hat{S}^\dagger |1'_{\pm}\rangle |\{v_j\}\rangle_{\text{vib}}$, where $\{v_j\}$ is a set of occupation numbers for the vibrational modes of the solvent-SMM system. These magnetic polarons can be thought as magnetic electronic states strongly coupled to a distortion of the molecular geometry. They inherit the magnetic properties of the corresponding electronic states, and can be seen as the molecu-

lar equivalent of the magnetic polarons observed in a range of magnetic materials [28–30]. Polaron representations of vibronic systems have been employed in a wide variety of settings, ranging from spin-boson models [27, 31] to photosynthetic complexes [32–34], to quantum dots [35–37], providing a convenient basis to describe the dynamics of quantum systems strongly coupled to a vibrational environment. These methods are particularly well suited for condensed matter systems where the electron-phonon coupling is strong but causes very slow transitions between different electronic states, allowing exact treatment of the pure-dephasing part of the electron-phonon coupling and renormalising the electronic parameters. For this reason, the polaron transformation is especially effective for describing our system (as detailed in Section S3). The most striking advantage of this approach is that the average effect of the spin-phonon coupling is included non-perturbatively into the electronic part of the Hamiltonian, leaving behind a vanishingly small residual spin-phonon coupling.

As a last step, we bring the Hamiltonian in Eq. (7) into a more familiar form by expressing it in terms of an effective g -matrix. We recall that the quantities Δ_1 and \mathbf{w}_j depend linearly on the magnetic field \mathbf{B} via the Zeeman Hamiltonian \hat{H}_{Zee} . An additional dependence on the orientation of the magnetic field comes from the mixing angles θ_1 and ϕ_1 introduced in Eqs. (2) and (3), appearing in the states $|1_{\pm}\rangle$ used in the definition of \mathbf{w}_j . This further dependence is removed by transforming the Pauli operators back to the basis $\{|1\rangle, |\bar{1}\rangle\}$ via a three-dimensional rotation $\sigma = \mathbf{R}_{\theta_1, \phi_1} \cdot \sigma''$. Finally, we obtain

$$\hat{H}_{\text{eff}}^{(\text{pol})} = E_1 + \mu_B \mathbf{B} \cdot \left(\mathbf{g}^{\text{el}} + \sum_j \mathbf{g}_j^{\text{vib}} \right) \cdot \frac{\sigma}{2}, \quad (8)$$

for appropriately defined electronic and single-mode vibronic g -matrices \mathbf{g}^{el} and $\mathbf{g}_j^{\text{vib}}$. These are directly related to the electronic splitting term Δ_1 and to the vibronic corrections described by \mathbf{w}_j in Eq. (7), respectively (see Section S2 for a thorough derivation). The main advantage of representing the ground Kramers doublet with an effective spin one-half Hamiltonian is that it provides a conceptually simple foundation for studying low-temperature magnetic behaviour of the complex, confining all microscopic details, including vibronic effects, to an effective g -matrix.

III. RESULTS

We begin by considering the influence of vibrations on the Zeeman splitting of the lowest doublet. The Zeeman splitting in absence of vibrations is simply given by $\Delta_1 = \mu_B |\mathbf{B} \cdot \mathbf{g}^{\text{el}}|$. In the presence of vibrations, the electronic g -matrix \mathbf{g}^{el} is modified by adding the vibronic correction $\sum_j \mathbf{g}_j^{\text{vib}}$, resulting in the Zeeman splitting Δ_1^{vib} . In Fig. 2 we show the Zeeman splittings as a function of the orientation of the magnetic field \mathbf{B} , parametrised in terms of the polar angles (θ, ϕ) . Depending on the field orientation, vibrations can lead to either an increase or decrease of the Zeeman splitting. These

changes seem rather small when compared to the largest electronic splitting, obtained when \mathbf{B} is oriented along the z -axis (Fig. 1a), as expected for a complex with easy-axis anisotropy. However, they become quite significant for field orientations close to the xy -plane, where the purely electronic splitting Δ_1 becomes vanishingly small and Δ_1^{vib} can be dominated by the vibronic contribution. This is clearly shown in Fig. 2b and 2c, where we decompose the total field $\mathbf{B} = \mathbf{B}_{\text{int}} + \mathbf{B}_{\text{ext}}$ in a fixed internal component \mathbf{B}_{int} originating from dipolar and hyperfine interactions, responsible for opening a tunnelling gap, and an external part \mathbf{B}_{ext} which we sweep along a fixed direction across zero. We note that this effect is specific to states with easy-axis magnetic anisotropy, however this is the defining feature of SMMs, such that our results should be generally applicable to all Kramers SMMs. A more in-depth discussion on the origin and magnitude of the internal field can be found in Section S5. When these fields lie in the plane perpendicular to the purely electronic easy axis, i.e. the hard plane, the vibronic splitting can be four orders of magnitude larger than the electronic one (Fig. 2b). The situation is reversed when the fields lie in the hard plane of the vibronic g -matrix (Fig. 2c).

So far we have seen that spin-phonon coupling can either enhance or reduce the tunnelling gap in the presence of a magnetic field depending on its orientation. For this reason, it is not immediately clear whether its effects survive ensemble averaging in a collection of randomly oriented SMMs, such as the frozen solutions considered in magnetometry experiments. In order to check this, let us consider an ideal field-dependent magnetisation measurement. When sweeping a magnetic field B_{ext} at a constant rate from positive to negative values along a given direction, QTM is typically observed as a sharp step in the magnetisation of the sample when crossing the region around $B_{\text{ext}} = 0$ [10]. This sudden change of the magnetisation is due to a non-adiabatic spin-flip transition between the two lowest energy spin states, that occurs when traversing an avoided crossing (see diagram in Fig. 1b, right). The spin-flip probability is given by the celebrated Landau-Zener expression [38–43], which in our case takes the form

$$P_{\text{LZ}} = 1 - \exp\left(-\frac{\pi |\Delta_{\perp}|^2}{2|\mathbf{v}|}\right), \quad (9)$$

where we have defined $\mathbf{v} = \mu_B d\mathbf{B}_{\text{ext}}/dt \cdot \mathbf{g}$, and Δ_{\perp} is the component of $\Delta = \mu_B \mathbf{B}_{\text{int}} \cdot \mathbf{g}$ perpendicular to \mathbf{v} , while \mathbf{g} denotes the total electronic-vibronic g -matrix appearing in Eq. (8) (see Section S2 for a derivation of Eq. (9)). We account for orientational disorder by averaging Eq. (9) over all possible orientations of internal and external magnetic fields, yielding the ensemble average $\langle P_{\text{LZ}} \rangle$.

The effect of spin-phonon coupling on the spin-flip dynamics of an ensemble of SMMs can be clearly seen in Fig. 3. Including the vibronic correction to the ground doublet g -matrix leads to enhanced spin-flip probabilities across a wide range of internal field strengths and field sweep rates. This is in line with previous results suggesting that molecular flexibility correlates with QTM [22]. To further corroborate our model, we test its predictions against experimental data. We extracted the average spin-flip probability from published hysteresis data

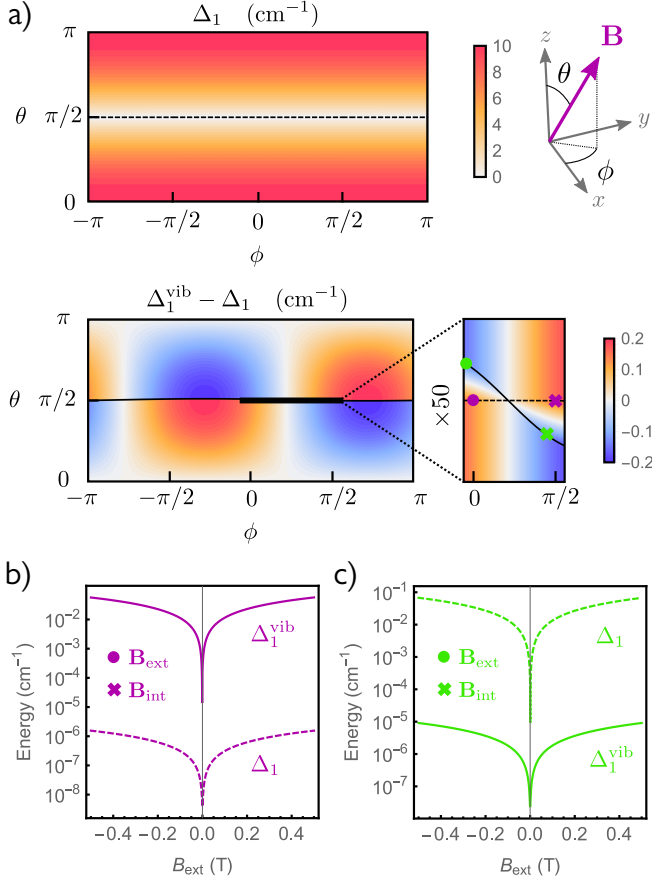


FIG. 2. **Zeeman splitting of the ground Kramers doublet.** (a) Electronic ground doublet splitting (Δ_1 , top) and vibronic correction ($\Delta_1^{\text{vib}} - \Delta_1$, bottom) as a function of the orientation of the magnetic field $\mathbf{B} = (\sin \theta \cos \phi, \sin \theta \sin \phi, \cos \theta)$, with magnitude fixed to 1 T. The dashed (solid) line corresponds to the electronic (vibronic) hard plane. (b–c) Electronic (dashed) and vibronic (solid) Zeeman splitting of the ground doublet as a function of the external field magnitude B_{ext} in the presence of a transverse internal field $B_{\text{int}} = 1$ mT. External and internal fields are perpendicular to each other and were both chosen to lie in the hard plane of either the electronic (b) or vibronic (c) g -matrix. The orientation of the external (internal) field is shown for both cases as circles (crosses) in the inset in (a), with colors matching the ones in (b) and (c).

of $[\text{Dy}(\text{Cp}^{\text{tt}})_2][\text{B}(\text{C}_6\text{F}_5)_4]$ in DCM with sweep rates ranging between 10–20 Oe/s [6], yielding a value of $\langle P_{\text{LZ}} \rangle = 0.27$, indicated by the pink line in Fig. 3. We then checked what strength of the internal field B_{int} is required to reproduce such spin-flip probability based on Eq. (9). In Fig. 3, we observe that the values of B_{int} required by the vibronic model to reproduce the observed spin-flip probability are perfectly consistent with the dipolar fields naturally occurring in the sample, whereas the purely electronic model necessitates internal fields that are one order of magnitude larger. These results clearly demonstrate the significance of spin-phonon coupling for QTM in a disordered ensemble of SMMs. A detailed discussion on the estimation of spin-flip probabilities and internal fields from magnetisation measurements is presented in Sec-

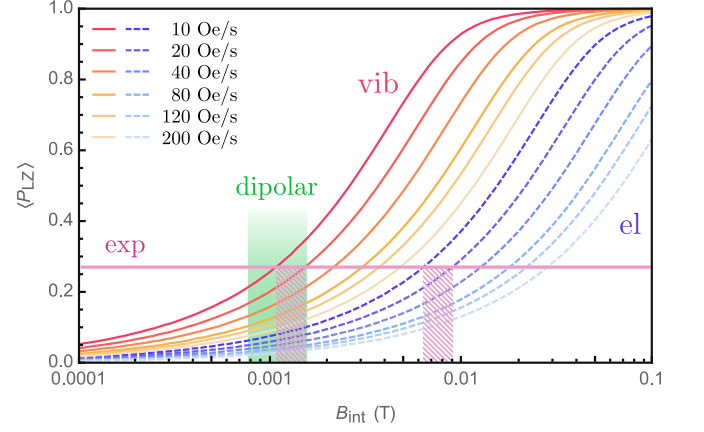


FIG. 3. **Landau-Zener spin-flip probability.** Ensemble-averaged spin-flip probability as a function of the internal field strength B_{int} causing tunnelling within the ground Kramers doublet, shown for different sweep rates dB_{ext}/dt . Results for the vibronic model of Eq. (8) are shown as orange solid lines, together with the spin-flip probabilities predicted by a purely electronic model obtained by setting the spin-phonon coupling to zero, shown as blue dashed lines. The horizontal pink line indicates $\langle P_{\text{LZ}} \rangle = 0.27$, extracted from hysteresis data from Ref. [6] (Section S4). The green shaded area indicates the range of values for typical dipolar fields in the corresponding sample (Section S5).

tions S4 and S5.

IV. DISCUSSION

As shown above, the combined effect of all vibrations in a randomly oriented ensemble of solvated SMMs is to enhance QTM. However, not all vibrations contribute to the same extent. Based on the polaron model introduced above, vibrations with large spin-phonon coupling and low frequency have a larger impact on the magnetic properties of the ground Kramers doublet. This can be seen from Eq. (7), where the vibronic correction to the effective ground Kramers Hamiltonian is weighted by the factor $\langle 1|\hat{V}_j|1\rangle/\omega_j$. Another property of vibrations that can influence QTM is their symmetry. In monometallic SMMs, QTM has generally been correlated with a reduction of the axial symmetry of the complex, either by the presence of flexible ligands or by transverse magnetic fields. Since we are interested in symmetry only as long as it influences magnetism, it is useful to introduce a measure of axiality on the g -matrix, such as

$$A(\mathbf{g}) = \frac{\|\mathbf{g} - \frac{1}{3}\text{Tr } \mathbf{g}\|}{\sqrt{\frac{2}{3}\text{Tr } \mathbf{g}}}, \quad (10)$$

where $\|\cdot\|$ denotes the Frobenius norm. This measure yields 1 for a perfect easy-axis complex, 1/2 for an easy plane system, and 0 for the perfectly isotropic case. The axiality of an individual vibrational mode can be quantified as $A_j = A(\mathbf{g}^{\text{el}} + \mathbf{g}_j^{\text{vib}})$ by building a single-mode vibronic g -matrix, analogous to

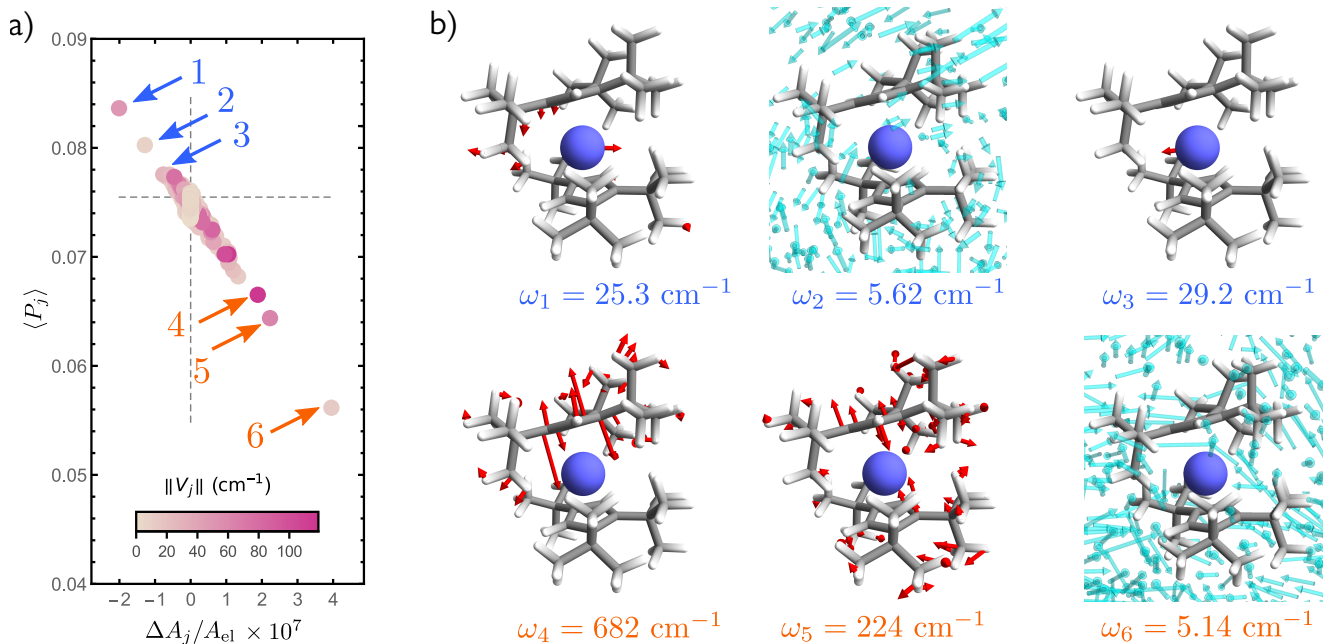


FIG. 4. **Single-mode contributions to tunnelling of the magnetisation.** (a) Single-mode vibronic Landau-Zener probabilities plotted for each vibrational mode, shown as a function of the mode axiality relative to the axiality of the purely electronic g -matrix ($\Delta A_j = A_j - A_{el}$). The magnitude of the internal field is fixed to $B_{int} = 1$ mT and the external field sweep rate is 10 Oe/s. The color coding represents the spin-phonon coupling strength $\|\hat{V}_j\|$. Grey dashed lines corresponds to the purely electronic model. (b) Visual representation of the displacements induced by the vibrational modes indicated by arrows in (a). Solvent motion is only shown for modes 2 and 6, which have negligible amplitude on the SMM.

the multi-mode one introduced in Eq. (8). We might be tempted to intuitively conclude that vibrational motion always decreases the axiality with respect to its electronic value $A_{el} = A(\mathbf{g}^{el})$, given that the collective effect of vibrations is to enhance QTM. However, when considered individually, some vibrations can have the opposite effect, of effectively increasing the magnetic axiality.

In order to see how axiality correlates to QTM, we calculate the single-mode Landau-Zener probabilities $\langle P_j \rangle$. These are obtained by replacing the multi-mode vibronic g -matrix in Eq. (8) with the single-mode one $\mathbf{g}^{el} + \mathbf{g}_j^{vib}$, and following the same procedure detailed in Section S2. The single-mode contribution to the spin-flip probability unambiguously correlates with mode axiality, as shown in Fig. 4a. Vibrational modes that lead to a larger QTM probability are likely to reduce the magnetic axiality of the complex (top-left sector). Vice versa, those vibrational modes that enhance axiality also suppress QTM (bottom-right sector).

As a first step towards uncovering the microscopic basis of this unexpected behaviour, we single out the three vibrational modes that have the largest impact on axiality and spin-flip probability in both directions. These vibrational modes, labelled 1–6, represent a range of qualitatively distinct vibrations, as can be observed in Fig. 4b. Modes 4 and 5 are among the ones exhibiting the strongest spin-phonon coupling. Both of them are mainly localised on one of the Cp^{III} ligands and involve atomic displacements along the easy axis and, to a lesser extent, rotations of the methyl groups. Modes 1 and 3 are among the ones with largest amplitude on the Dy ion,

which in both cases mainly moves in the hard plane, disrupting axial symmetry and enhancing tunnelling. Lastly, modes 2 and 6 predominantly correspond to solvent vibrations, and are thus very low energy and so give a large contribution via the small denominator in Eq. (7).

This analysis shows that the effect of vibrational modes on QTM is more nuanced than what both intuition and previous work would suggest. Despite leading to an overall increase of the spin-flip probability on average, coupling the spin to specific vibrations can increase the magnetic axiality of the complex and suppress QTM. This opens a new avenue for the improvement of magnetic relaxation times in SMMs, shifting the role of vibrations from purely antagonistic to potentially beneficial.

According to the results shown above, the ideal candidates to observe vibronic suppression of QTM are systems exhibiting strongly axial, low frequency vibrations, strongly coupled to the electronic effective spin. Strong spin-phonon coupling and low frequency ensure a significant change in magnetic properties according to Eq. (7), but may not be enough to hinder tunnelling. In order to be beneficial, vibrations also need to enhance the axiality of the ground doublet g -matrix. The relation between magnetic axiality and vibrational symmetry remains yet to be explored, and might lead to new insights regarding rational design of ideal ligands.

V. CONCLUSIONS

In conclusion, we have presented a detailed description of the effect of molecular and solvent vibrations on the quantum tunnelling between low-energy spin states in a single-ion Dy(III) SMM. Our theoretical results, based on an *ab initio* approach, are complemented by a polaron treatment of the relevant vibronic degrees of freedom, which does not suffer from any weak spin-phonon coupling assumption and is therefore well-suited to other strong coupling scenarios. We have been able to derive a non-perturbative vibronic correction to the effective g -matrix of the lowest-energy Kramers doublet, which we have used as a basis to determine the tunnelling dynamics in a magnetic field sweep experiment. This has allowed us to formulate the key observation that, vibrations collectively enhance QTM, but some particular vibrational modes unexpectedly suppress QTM. This behaviour correlates to the axially of each mode, which can be used as a proxy for determining whether a specific vibration enhances or hinders tunnelling.

The observation that individual vibrational modes can suppress QTM challenges the paradigm that dismisses vibrations as detrimental, a mere obstacle to achieving long-lasting information storage on SMMs, and forces us instead to reconsider them under a new light, as tools that can be actively engineered to our advantage to keep tunnelling at bay and extend relaxation timescales in molecular magnets. This idea suggests parallelisms with other seemingly unrelated chem-

ical systems where electron-phonon coupling plays an important role. For example, the study of electronic energy transfer across photosynthetic complexes was radically transformed by the simple observation that vibrations could play an active role, maintaining quantum coherence in noisy room-temperature environments, rather than just passively causing decoherence between electronic states [44]. Identifying these beneficial vibrations and amplifying their effect via chemical design of new SMMs remains an open question, whose solution we believe could greatly benefit from the results and the methods introduced in this work.

ACKNOWLEDGEMENTS

This work was made possible thanks to the ERC grant 2019-STG-851504 and Royal Society fellowship URF191320. The authors also acknowledge support from the Computational Shared Facility at the University of Manchester.

DATA AVAILABILITY

The data that support the findings of this study are available at <http://doi.org/10.48420/21892887>.

-
- [1] M. N. Leuenberger and D. Loss, *Quantum computing in molecular magnets*, Nature **410**, 789 (2001).
- [2] R. Sessoli, *Magnetic molecules back in the race*, Nature **548**, 400 (2017).
- [3] E. Coronado, *Molecular magnetism: from chemical design to spin control in molecules, materials and devices*, Nature Reviews Materials **5**, 87 (2020).
- [4] N. F. Chilton, *Molecular magnetism*, Annual Review of Materials Research **52**, 79 (2022).
- [5] R. Sessoli, D. Gatteschi, A. Caneschi, and M. A. Novak, *Magnetic bistability in a metal-ion cluster*, Nature **365**, 141 (1993).
- [6] C. A. P. Goodwin, F. Ortu, D. Reta, N. F. Chilton, and D. P. Mills, *Molecular magnetic hysteresis at 60 kelvin in dysprosocenium*, Nature **548**, 439 (2017).
- [7] F.-S. Guo, B. M. Day, Y.-C. Chen, M.-L. Tong, A. Mansikkamäki, and R. A. Layfield, *Magnetic hysteresis up to 80 kelvin in a dysprosium metallocene single-molecule magnet*, Science **362**, 1400 (2018).
- [8] C. A. Gould, K. R. McClain, D. Reta, J. G. C. Kragoskow, D. A. Marchiori, E. Lachman, E.-S. Choi, J. G. Analytis, R. D. Britt, N. F. Chilton, B. G. Harvey, and J. R. Long, *Ultrafast magnetism from mixed-valence dylanthanide complexes with metal-metal bonding*, Science **375**, 198 (2022).
- [9] D. Gatteschi, R. Sessoli, and J. Villain, *Molecular Nanomagnets* (Oxford University Press, 2006).
- [10] L. Thomas, F. Lioni, R. Ballou, D. Gatteschi, R. Sessoli, and B. Barbara, *Macroscopic quantum tunnelling of magnetization in a single crystal of nanomagnets*, Nature **383**, 145 (1996).
- [11] D. A. Garanin and E. M. Chudnovsky, *Thermally activated resonant magnetization tunneling in molecular magnets: Mn₁₂ac and others*, Phys. Rev. B **56**, 11102 (1997).
- [12] D. Reta, J. G. C. Kragoskow, and N. F. Chilton, *Ab initio prediction of high-temperature magnetic relaxation rates in single-molecule magnets*, Journal of the American Chemical Society **143**, 5943 (2021).
- [13] M. Briganti, F. Santanni, L. Tesi, F. Totti, R. Sessoli, and A. Lunghi, *A complete ab initio view of Orbach and Raman spin-lattice relaxation in a dysprosium coordination compound*, Journal of the American Chemical Society **143**, 13633 (2021).
- [14] J. K. Staab and N. F. Chilton, *Analytic linear vibronic coupling method for first-principles spin-dynamics calculations in single-molecule magnets*, Journal of Chemical Theory and Computation (2022), 10.1021/acs.jctc.2c00611.
- [15] A. Lunghi, *Toward exact predictions of spin-phonon relaxation times: An ab initio implementation of open quantum systems theory*, Science Advances **8**, eabn7880 (2022).
- [16] K. Irländer and J. Schnack, *Spin-phonon interaction induces tunnel splitting in single-molecule magnets*, Phys. Rev. B **102**, 054407 (2020).
- [17] K. Irländer, H.-J. Schmidt, and J. Schnack, *Supersymmetric spin-phonon coupling prevents odd integer spins from quantum tunneling*, The European Physical Journal B **94**, 68 (2021).
- [18] A. H. Kramers, *Théorie générale de la rotation paramagnétique dans les cristaux*, Proceedings Royal Acad. Amsterdam **33**, 959 (1930).
- [19] N. Ishikawa, M. Sugita, and W. Wernsdorfer, *Quantum tunneling of magnetization in lanthanide single-molecule magnets: Bis(phthalocyaninato)terbium and bis(phthalocyaninato)dysprosium anions*, Angewandte Chemie International Edition **44**, 2931 (2005).

- [20] E. Moreno-Pineda, M. Damjanović, O. Fuhr, W. Wernsdorfer, and M. Ruben, *Nuclear spin isomers: Engineering a $\text{Et}_4\text{N}[\text{DyPc}_2]$ spin qudit*, *Angewandte Chemie International Edition* **56**, 9915 (2017).
- [21] N. F. Chilton, S. K. Langley, B. Moubaraki, A. Soncini, S. R. Batten, and K. S. Murray, *Single molecule magnetism in a family of mononuclear β -diketonate lanthanide(III) complexes: rationalization of magnetic anisotropy in complexes of low symmetry*, *Chem. Sci.* **4**, 1719 (2013).
- [22] F. Ortu, D. Reta, Y.-S. Ding, C. A. P. Goodwin, M. P. Gregson, E. J. L. McInnes, R. E. P. Winpenny, Y.-Z. Zheng, S. T. Liddle, D. P. Mills, and N. F. Chilton, *Studies of hysteresis and quantum tunnelling of the magnetisation in dysprosium(III) single molecule magnets*, *Dalton Trans.* **48**, 8541 (2019).
- [23] F. Pointillart, K. Bernot, S. Golhen, B. Le Guennic, T. Guizouarn, L. Ouahab, and O. Cador, *Magnetic memory in an isotopically enriched and magnetically isolated mononuclear dysprosium complex*, *Angewandte Chemie International Edition* **54**, 1504 (2015).
- [24] Y. Kishi, F. Pointillart, B. Lefeuvre, F. Riobé, B. Le Guennic, S. Golhen, O. Cador, O. Maury, H. Fujiwara, and L. Ouahab, *Isotopically enriched polymorphs of dysprosium single molecule magnets*, *Chem. Commun.* **53**, 3575 (2017).
- [25] J. Flores Gonzalez, F. Pointillart, and O. Cador, *Hyperfine coupling and slow magnetic relaxation in isotopically enriched Dy^{III} mononuclear single-molecule magnets*, *Inorg. Chem. Front.* **6**, 1081 (2019).
- [26] E. Moreno-Pineda, G. Taran, W. Wernsdorfer, and M. Ruben, *Quantum tunnelling of the magnetisation in single-molecule magnet isotopologue dimers*, *Chem. Sci.* **10**, 5138 (2019).
- [27] R. Silbey and R. A. Harris, *Variational calculation of the dynamics of a two level system interacting with a bath*, *The Journal of Chemical Physics* **80**, 2615 (1984).
- [28] D. R. Yakovlev and W. Ossau, *Magnetic polarons*, in *Introduction to the Physics of Diluted Magnetic Semiconductors*, edited by J. A. Gaj and J. Kossut (Springer Berlin Heidelberg, Berlin, Heidelberg, 2010) pp. 221–262.
- [29] S. Schott, U. Chopra, V. Lemaure, A. Melnyk, Y. Olivier, R. Di Pietro, I. Romanov, R. L. Carey, X. Jiao, C. Jellett, M. Little, A. Marks, C. R. McNeill, I. McCulloch, E. R. McNellis, D. Andrienko, D. Beljonne, J. Sinova, and H. Siringhaus, *Polaron spin dynamics in high-mobility polymeric semiconductors*, *Nature Physics* **15**, 814 (2019).
- [30] F. Godejohann, A. V. Scherbakov, S. M. Kukhtaruk, A. N. Poddubny, D. D. Yaremkevich, M. Wang, A. Nadzeyka, D. R. Yakovlev, A. W. Rushforth, A. V. Akimov, and M. Bayer, *Magnon polaron formed by selectively coupled coherent magnon and phonon modes of a surface patterned ferromagnet*, *Phys. Rev. B* **102**, 144438 (2020).
- [31] A. W. Chin, J. Prior, S. F. Huelga, and M. B. Plenio, *Generalized polaron ansatz for the ground state of the sub-ohmic spin-boson model: An analytic theory of the localization transition*, *Phys. Rev. Lett.* **107**, 160601 (2011).
- [32] L. Yang, M. Devi, and S. Jang, *Polaronic quantum master equation theory of inelastic and coherent resonance energy transfer for soft systems*, *The Journal of Chemical Physics* **137**, 024101 (2012).
- [33] A. Kolli, A. Nazir, and A. Olaya-Castro, *Electronic excitation dynamics in multichromophoric systems described via a polaron-representation master equation*, *The Journal of Chemical Physics* **135**, 154112 (2011).
- [34] F. A. Pollock, D. P. S. McCutcheon, B. W. Lovett, E. M. Gauger, and A. Nazir, *A multi-site variational master equation approach to dissipative energy transfer*, *New Journal of Physics* **15**, 075018 (2013).
- [35] I. Wilson-Rae and A. Imamoglu, *Quantum dot cavity-QED in the presence of strong electron-phonon interactions*, *Phys. Rev. B* **65**, 235311 (2002).
- [36] D. P. S. McCutcheon and A. Nazir, *Quantum dot Rabi rotations beyond the weak exciton-phonon coupling regime*, *New Journal of Physics* **12**, 113042 (2010).
- [37] A. Nazir and D. P. S. McCutcheon, *Modelling exciton-phonon interactions in optically driven quantum dots*, *Journal of Physics: Condensed Matter* **28**, 103002 (2016).
- [38] L. D. Landau, *Zur Theorie der Energieübertragung*, *Phys. Z. Sowjetunion* **1**, 88 (1932).
- [39] L. D. Landau, *Zur Theorie der Energieübertragung II*, *Phys. Z. Sowjetunion* **2**, 46 (1932).
- [40] C. Zener and R. H. Fowler, *Non-adiabatic crossing of energy levels*, *Proceedings of the Royal Society of London. Series A* **137**, 696 (1932).
- [41] E. C. G. Stückelberg, *Theorie der unelastischen Stöße zwischen Atomen*, *Helv. Phys. Acta* **5**, 369 (1932).
- [42] E. Majorana, *Atomi orientati in campo magnetico variabile*, *Il Nuovo Cimento* **9**, 43 (1932).
- [43] O. V. Ivakhnenko, S. N. Shevchenko, and F. Nori, *Nonadiabatic Landau-Zener-Stückelberg-Majorana transitions, dynamics, and interference*, *Physics Reports* **995**, 1 (2023).
- [44] G. D. Scholes, G. R. Fleming, L. X. Chen, A. Aspuru-Guzik, A. Buchleitner, D. F. Coker, G. S. Engel, R. van Grondelle, A. Ishizaki, D. M. Jonas, J. S. Lundeen, J. K. McCusker, S. Mukamel, J. P. Ogilvie, A. Olaya-Castro, M. A. Ratner, F. C. Spano, K. B. Whaley, and X. Zhu, *Using coherence to enhance function in chemical and biophysical systems*, *Nature* **543**, 647 (2017).

Supplementary Information:

Vibronic Effects on the Quantum Tunnelling of Magnetisation in Single-Molecule Magnets

Andrea Mattioni,^{1,*} Jakob K. Staab,¹ William J. A. Blackmore,¹ Daniel Reta,^{1,2}
Jake Iles-Smith,^{3,4} Ahsan Nazir,³ and Nicholas F. Chilton^{1,†}

¹*Department of Chemistry, School of Natural Sciences,
The University of Manchester, Oxford Road, Manchester, M13 9PL, UK*

²*Faculty of Chemistry, UPV/EHU & Donostia International Physics Center DIPC,
Ikerbasque, Basque Foundation for Science, Bilbao, Spain*

³*Department of Physics and Astronomy, School of Natural Sciences,
The University of Manchester, Oxford Road, Manchester M13 9PL, UK*

⁴*Department of Electrical and Electronic Engineering, School of Engineering,
The University of Manchester, Sackville Street Building, Manchester M1 3BB, UK*

* andrea.mattioni@manchester.ac.uk

† nicholas.chilton@manchester.ac.uk

S1. AB INITIO CALCULATIONS

The ab initio model of the DCM-solvated $[\text{Dy}(\text{Cp}^{\text{ttt}})_2]^+$ molecule is constructed using a multi-layer approach. During geometry optimisation and frequency calculation the system is partitioned into two layers following the ONIOM scheme [1]. The high-level layer, consisting of the SMM itself and the first solvation shell of 26 DCM molecules, is described by Density Functional Theory (DFT) while the outer bulk of the DCM ball constitutes the low-level layer modelled by the semi-empirical PM6 method. All DFT calculations are carried out using the pure PBE exchange-correlation functional [2] with Grimme's D3 dispersion correction. Dysprosium is replaced by its diamagnetic analogue yttrium for which the Stuttgart RSC 1997 ECP basis is employed [3]. Cp ring carbons directly coordinated to the central ion are equipped with Dunning's correlation consistent triple-zeta polarised cc-pVTZ basis set and all remaining atoms with its double-zeta analogue cc-pVDZ [4]. Subsequently, the electronic spin states and spin-phonon coupling parameters are calculated at the CASSCF-SO level explicitly accounting for the strong static correlation present in the f-shell of Dy(III) ions. At this level, environmental effects are treated using an electrostatic point charge representation of all DCM atoms. All DFT/PM6 calculations are carried out with GAUSSIAN version 9 revision D.01 [5] and the CASSCF calculations are carried out with OPENMOLCAS version 21.06 [6].

The starting $[\text{Dy}(\text{Cp}^{\text{ttt}})_2]^+$ solvated system was obtained using the solvate program belonging to the AmberTool suite of packages, with box as method and CHCL3BOX as solvent model. Chloroform molecules were subsequently converted to DCM. From this large system, only molecules falling within 9 Å from the central metal atom are considered from now on. The initial disordered system of 160 DCM molecules packed around the $[\text{Dy}(\text{Cp}^{\text{ttt}})_2]^+$ crystal structure [7] is pre-optimised in steps, starting by only optimising the high-level layer atoms and freezing the rest of the system. The low-layer atoms are pre-optimised along the same lines starting with DCM molecules closest to the SMM and working in shells towards the outside. Subsequently, the whole system is geometry optimised until RMS (maximum) values in force and displacement corresponding to 0.00045 au (0.0003 au) and 0.0018 au (0.0012 au) are reached, respectively. After adjusting the isotopic mass of yttrium to that of dysprosium $m_{\text{Dy}} = 162.5\text{u}$, vibrational normal modes and frequencies of the entire molecular aggregate are computed within the harmonic approximation.

Electrostatic atomic point charge representations of the environment DCM molecules are evaluated for each isolated solvent molecule independently at the DFT level of theory employing the CHarges from ELectrostatic Potentials using a Grid-based (ChelpG) method [8], which serve as a classical model of environmental effects in the subsequent CASSCF calculations.

The evaluation of equilibrium electronic states and spin-phonon coupling parameters is carried out at the CASSCF level including scalar relativistic effects using the second-order Douglas-Kroll Hamiltonian and spin-orbit coupling through the atomic mean field approximation implemented in the restricted active space state interaction approach [9, 10]. The dysprosium atom is equipped with the ANO-RCC-VTZP, the Cp ring carbons with the ANO-RCC-VDZP and the remaining atoms with the ANO-RCC-VDZ basis set [11]. The resolution of the identity approximation with an on-the-fly acCD auxiliary basis is employed to handle the two-electron integrals [12]. The active space of 9 electrons in 7 orbitals, spanned by 4f atomic orbitals, is employed in a state-average CASSCF calculation including the 18 lowest lying sextet roots which span the ${}^6\text{H}$ and ${}^6\text{F}$ atomic terms.

We use our own implementation of spin Hamiltonian parameter projection to obtain the crystal field parameters B_k^q entering the Hamiltonian

$$\hat{H}_{\text{CF}} = \sum_{k=2,4,6} \sum_{q=-k}^k \theta_k B_k^q O_k^q(\hat{\mathbf{J}}), \quad (\text{S1})$$

describing the ${}^6\text{H}_{15/2}$ ground state multiplet. Operator equivalent factors and Stevens operators are denoted by θ_k and $O_k^q(\hat{\mathbf{J}})$, where $\hat{\mathbf{J}} = (\hat{J}_x, \hat{J}_y, \hat{J}_z)$ are the angular momentum components. Spin-phonon coupling arises from changes to the Hamiltonian (S1) due to slight distortions of the molecular geometry, parametrised as

$$B_k^q(\{X_j\}) = B_k^q + \sum_{j=1}^M \frac{\partial B_k^q}{\partial X_j} X_j + \dots, \quad (\text{S2})$$

where X_j denotes the dimensionless j -th normal coordinate of the complex under consideration. The derivatives $\partial B_k^q / \partial X_j$ are calculated using the Linear Vibronic Coupling (LVC) approach described in Ref. [13] based on the state-average CASSCF density-fitting gradients and non-adiabatic coupling involving all 18 sextet roots.

The final step leading to Eq. (1) in the main text is to quantise the normal modes and express them in terms of bosonic annihilation and creation operators satisfying $[\hat{b}_i, \hat{b}_j^\dagger] = \delta_{ij}$ as

$$\hat{X}_j = \frac{\hat{b}_j + \hat{b}_j^\dagger}{\sqrt{2}}. \quad (\text{S3})$$

Defining the spin-phonon coupling operators

$$\hat{V}_j = \frac{1}{\sqrt{2}} \sum_{k,q} \theta_k \frac{\partial B_k^q}{\partial X_j} O_k^q(\hat{\mathbf{J}}), \quad (\text{S4})$$

we can finally write down the crystal field Hamiltonian including linear spin-phonon coupling as

$$\hat{H} = \hat{H}_{\text{CF}} + \sum_j \hat{V}_j \otimes (\hat{b}_j + \hat{b}_j^\dagger) + \sum_j \omega_j \hat{b}_j^\dagger \hat{b}_j. \quad (\text{S5})$$

S2. DERIVATION OF THE EFFECTIVE VIBRONIC DOUBLET HAMILTONIAN

A. Electronic perturbation Theory

The starting point for our analysis of vibronic effects on QTM is the vibronic Hamiltonian

$$\hat{H} = \sum_{m>0} E_m (|m\rangle\langle m| + |\bar{m}\rangle\langle\bar{m}|) + \hat{H}_{Zee} + \sum_j \hat{V}_j \otimes (\hat{b}_j + \hat{b}_j^\dagger) + \sum_j \omega_j \hat{b}_j^\dagger \hat{b}_j, \quad (\text{S6})$$

where $\hat{H}_{Zee} = \mu_B g_J \mathbf{B} \cdot \hat{\mathbf{J}}$ is the Zeeman interaction with a magnetic field \mathbf{B} . The doubly degenerate eigenstates of the crystal field Hamiltonian $H_{CF} = \sum_{m>0} E_m (|m\rangle\langle m| + |\bar{m}\rangle\langle\bar{m}|)$ are related by time-reversal symmetry, i.e. $\hat{\Theta}|m\rangle \propto |\bar{m}\rangle$ with $\hat{\Theta}^2|m\rangle = -|m\rangle$, where $\hat{\Theta}$ is the time-reversal operator. In the case of $[\text{Dy}(\text{Cp}^{\text{tt}})_2]^+$, the total electronic angular momentum is $J = 15/2$, leading to $2J + 1 = 16$ electronic states. We label these states in ascending energy with integers $m = \pm 1, \dots, \pm 8$, using the compact notation $|-m\rangle = |\bar{m}\rangle$.

We momentarily neglect the spin-phonon coupling and focus on the purely electronic Hamiltonian $H_{el} = H_{CF} + H_{Zee}$. Within each degenerate subspace, the Zeeman term selects a specific electronic basis and lifts its degeneracy. This can be seen by projecting the electronic Hamiltonian onto the m -th subspace and diagonalising the 2×2 matrix

$$H_{el}^{(m)} = E_m + \mu_B g_J \begin{pmatrix} \langle m|\mathbf{B} \cdot \hat{\mathbf{J}}|m\rangle & \langle m|\mathbf{B} \cdot \hat{\mathbf{J}}|\bar{m}\rangle \\ \langle \bar{m}|\mathbf{B} \cdot \hat{\mathbf{J}}|m\rangle & \langle \bar{m}|\mathbf{B} \cdot \hat{\mathbf{J}}|\bar{m}\rangle \end{pmatrix}. \quad (\text{S7})$$

For each individual cartesian component of the angular momentum, we decompose the corresponding 2×2 matrix in terms of Pauli spin operators, which allows to rewrite the Hamiltonian of the m -th doublet as $H_{el}^{(m)} = E_m + \mu_B \mathbf{B} \cdot \mathbf{g}_{el}^{(m)} \cdot \boldsymbol{\sigma}^{(m)}/2$, where

$$\mathbf{g}_{el}^{(m)} = 2g_J \begin{pmatrix} \Re\langle \bar{m}|\hat{J}_x|m\rangle & \Im\langle \bar{m}|\hat{J}_x|m\rangle & \langle m|\hat{J}_x|m\rangle \\ \Re\langle \bar{m}|\hat{J}_y|m\rangle & \Im\langle \bar{m}|\hat{J}_y|m\rangle & \langle m|\hat{J}_y|m\rangle \\ \Re\langle \bar{m}|\hat{J}_z|m\rangle & \Im\langle \bar{m}|\hat{J}_z|m\rangle & \langle m|\hat{J}_z|m\rangle \end{pmatrix} \quad (\text{S8})$$

is the g -matrix for an effective spin 1/2 and $\boldsymbol{\sigma}^{(m)} = (\sigma_x^{(m)}, \sigma_y^{(m)}, \sigma_z^{(m)})$, with $\sigma_z^{(m)} = |m\rangle\langle m| - |\bar{m}\rangle\langle\bar{m}|$. We note that in general the g -matrix in Eq. (S8) is not hermitean, but can be brought to such form by transforming the spin operators $\boldsymbol{\sigma}^{(m)}$ to an appropriate basis [14]. An easier prescription to find the hermitean form of any g -matrix \mathbf{g} is to redefine it as $\sqrt{\mathbf{g}\mathbf{g}^\dagger}$.

To lowest order in the magnetic field, the Zeeman interaction lifts the two-fold degeneracy by selecting the basis

$$|m_+\rangle = \cos\frac{\theta_m}{2}|m\rangle + e^{i\phi_m}\sin\frac{\theta_m}{2}|\bar{m}\rangle \quad (\text{S9})$$

$$|m_-\rangle = -\sin\frac{\theta_m}{2}|m\rangle + e^{i\phi_m}\cos\frac{\theta_m}{2}|\bar{m}\rangle \quad (\text{S10})$$

and shifting the energies according to $E_{m,\pm} = E_m \pm \Delta_m/2$, where the gap

$$\begin{aligned} \Delta_m &= \langle m_+|\hat{H}_{Zee}|m_+\rangle - \langle m_-|\hat{H}_{Zee}|m_-\rangle \\ &= 2\mu_B g_J \sqrt{\langle m|\mathbf{B} \cdot \hat{\mathbf{J}}|m\rangle^2 + |\langle m|\mathbf{B} \cdot \hat{\mathbf{J}}|\bar{m}\rangle|^2} \end{aligned} \quad (\text{S11})$$

can be obtained as the norm of the vector $\mathbf{j}_m = \mu_B \mathbf{B} \cdot \mathbf{g}_{el}^{(m)}$ and the phase and mixing angles are defined as

$$e^{i\phi_m} = \frac{\langle \bar{m}|\mathbf{B} \cdot \hat{\mathbf{J}}|m\rangle}{|\langle \bar{m}|\mathbf{B} \cdot \hat{\mathbf{J}}|m\rangle|}, \quad \tan\theta_m = \frac{|\langle \bar{m}|\mathbf{B} \cdot \hat{\mathbf{J}}|m\rangle|}{\langle m|\mathbf{B} \cdot \hat{\mathbf{J}}|m\rangle}, \quad (\text{S12})$$

or equivalently as the azimuthal and polar angles determining the direction of \mathbf{j}_m .

Besides selecting a preferred basis and lifting the degeneracy of each doublet, the Zeeman interaction also causes mixing between different doublets. In particular, the lowest doublet will change according to

$$|1'_\pm\rangle = |1_\pm\rangle + \sum_{m \neq 1, \bar{1}} |m\rangle \frac{\langle m|\hat{H}_{Zee}|1_\pm\rangle}{E_1 - E_m} + \mathcal{O}(B^2) \approx (1 - \hat{Q}_1 \hat{H}_{Zee}) |1_\pm\rangle, \quad (\text{S13})$$

with

$$\hat{Q}_1 = \sum_{m \neq 1, \bar{1}} |m\rangle \frac{1}{E_m - E_1} \langle m|. \quad (\text{S14})$$

B. Spin-boson Hamiltonian for the ground doublet

Now that we have an approximate expression for the relevant electronic states, we reintroduce the spin-phonon coupling into the picture. First, we project the vibronic Hamiltonian (S6) onto the subspace spanned by $|1'_\pm\rangle$, yielding

$$\hat{H}_{\text{eff}} = E_1 + \begin{pmatrix} \frac{\Delta_1}{2} & 0 \\ 0 & -\frac{\Delta_1}{2} \end{pmatrix} + \sum_j \begin{pmatrix} \langle 1'_+ | \hat{V}_j | 1'_+ \rangle & \langle 1'_+ | \hat{V}_j | 1'_- \rangle \\ \langle 1'_- | \hat{V}_j | 1'_+ \rangle & \langle 1'_- | \hat{V}_j | 1'_- \rangle \end{pmatrix} \otimes (\hat{b}_j + \hat{b}_j^\dagger) + \sum_j \omega_j \hat{b}_j^\dagger \hat{b}_j. \quad (\text{S15})$$

On this basis, the purely electronic part $\hat{H}_{\text{CF}} + \hat{H}_{\text{Zee}}$ is diagonal with eigenvalues $E_1 \pm \Delta_1/2$, and the purely vibrational part is trivially unaffected. On the other hand, the spin-phonon couplings can be calculated to lowest order in the magnetic field strength B as

$$\begin{aligned} \langle 1'_\pm | \hat{V}_j | 1'_\pm \rangle &= \langle 1_\pm | (1 - \hat{H}_{\text{Zee}} \hat{Q}_1) \hat{V}_j (1 - \hat{Q}_1 \hat{H}_{\text{Zee}}) | 1_\pm \rangle + \mathcal{O}(B^2) \\ &= \langle 1_\pm | \hat{V}_j | 1_\pm \rangle - \langle 1_\pm | (\hat{V}_j \hat{Q}_1 \hat{H}_{\text{Zee}} + \hat{H}_{\text{Zee}} \hat{Q}_1 \hat{V}_j) | 1_\pm \rangle + \mathcal{O}(B^2) \\ &= \langle 1 | \hat{V}_j | 1 \rangle - \langle 1_\pm | \hat{W}_j | 1_\pm \rangle + \mathcal{O}(B^2), \end{aligned} \quad (\text{S16})$$

$$\begin{aligned} \langle 1'_\mp | \hat{V}_j | 1'_\pm \rangle &= \langle 1_\mp | (1 - \hat{H}_{\text{Zee}} \hat{Q}_1) \hat{V}_j (1 - \hat{Q}_1 \hat{H}_{\text{Zee}}) | 1_\pm \rangle + \mathcal{O}(B^2) \\ &= \langle 1_\mp | \hat{V}_j | 1_\pm \rangle - \langle 1_\mp | (\hat{V}_j \hat{Q}_1 \hat{H}_{\text{Zee}} + \hat{H}_{\text{Zee}} \hat{Q}_1 \hat{V}_j) | 1_\pm \rangle + \mathcal{O}(B^2) \\ &= -\langle 1_\mp | \hat{W}_j | 1_\pm \rangle + \mathcal{O}(B^2), \end{aligned} \quad (\text{S17})$$

where we have defined

$$\hat{W}_j = \hat{V}_j \hat{Q}_1 \hat{H}_{\text{Zee}} + \hat{H}_{\text{Zee}} \hat{Q}_1 \hat{V}_j \quad (\text{S18})$$

and used the time-reversal invariance of the spin-phonon coupling operators to obtain $\langle 1_\pm | \hat{V}_j | 1_\pm \rangle = \langle 1 | \hat{V}_j | 1 \rangle$ and $\langle 1_\mp | \hat{V}_j | 1_\pm \rangle = 0$.

The two states $|1_\pm\rangle$ form a conjugate pair under time reversal, meaning that $\hat{\Theta} |1_\pm\rangle = \mp e^{i\alpha} |1_\mp\rangle$ for some $\alpha \in \mathbb{R}$. Using the fact that for any two states ψ, ϕ , and for any operator \hat{O} we have $\langle \psi | \hat{O} | \phi \rangle = \langle \hat{\Theta} \phi | \hat{\Theta} \hat{O}^\dagger \hat{\Theta}^{-1} | \hat{\Theta} \psi \rangle$, and recalling that the angular momentum operator is odd under time reversal, i.e. $\hat{\Theta} \hat{\mathbf{J}} \hat{\Theta}^{-1} = -\hat{\mathbf{J}}$, we can show that

$$\langle 1_- | \hat{W}_j | 1_- \rangle = \langle \hat{\Theta} 1_- | \hat{\Theta} \hat{W}_j \hat{\Theta}^{-1} | \hat{\Theta} 1_- \rangle = -\langle 1_+ | \hat{W}_j | 1_+ \rangle.$$

Keeping in mind these observations, and defining the vector

$$\mathbf{w}_j = \begin{pmatrix} w_j^x \\ w_j^y \\ w_j^z \end{pmatrix} = \begin{pmatrix} \Re \langle 1_- | \hat{W}_j | 1_+ \rangle \\ \Im \langle 1_- | \hat{W}_j | 1_+ \rangle \\ \langle 1_+ | \hat{W}_j | 1_+ \rangle \end{pmatrix}, \quad (\text{S19})$$

we can rewrite the spin-phonon coupling operators in Eq. (S15) as

$$\begin{pmatrix} \langle 1'_+ | \hat{V}_j | 1'_+ \rangle & \langle 1'_+ | \hat{V}_j | 1'_- \rangle \\ \langle 1'_- | \hat{V}_j | 1'_+ \rangle & \langle 1'_- | \hat{V}_j | 1'_- \rangle \end{pmatrix} = \langle 1 | \hat{V}_j | 1 \rangle - \begin{pmatrix} \langle 1_+ | \hat{W}_j | 1_+ \rangle & \langle 1_- | \hat{W}_j | 1_+ \rangle^* \\ \langle 1_- | \hat{W}_j | 1_+ \rangle & -\langle 1_+ | \hat{W}_j | 1_+ \rangle \end{pmatrix} = \langle 1 | \hat{V}_j | 1 \rangle - \mathbf{w}_j \cdot \boldsymbol{\sigma}' \quad (\text{S20})$$

where $\boldsymbol{\sigma}'$ is a vector whose entries are the Pauli matrices in the basis $|1'_\pm\rangle$, i.e. $\sigma'_z = |1'_+\rangle\langle 1'_+| - |1'_-\rangle\langle 1'_-|$. Plugging this back into Eq. (S15) and explicitly singling out the diagonal components of \hat{H}_{eff} in the basis $|1'_\pm\rangle$, we obtain

$$\begin{aligned} \hat{H}_{\text{eff}} &= |1'_+\rangle\langle 1'_+| \left[E_1 + \frac{\Delta_1}{2} + \sum_j \left(\langle 1 | \hat{V}_j | 1 \rangle - w_j^z \right) (\hat{b}_j + \hat{b}_j^\dagger) + \sum_j \omega_j \hat{b}_j^\dagger \hat{b}_j \right] \\ &+ |1'_-\rangle\langle 1'_-| \left[E_1 - \frac{\Delta_1}{2} + \sum_j \left(\langle 1 | \hat{V}_j | 1 \rangle + w_j^z \right) (\hat{b}_j + \hat{b}_j^\dagger) + \sum_j \omega_j \hat{b}_j^\dagger \hat{b}_j \right] \\ &- \sum_j \left(w_j^x \sigma'_x + w_j^y \sigma'_y \right) (\hat{b}_j + \hat{b}_j^\dagger). \end{aligned} \quad (\text{S21})$$

At this point, we apply a unitary polaron transformation to the Hamiltonian (S21)

$$\begin{aligned} \hat{S} &= \exp \left[\sum_{s=\pm} |1'_s\rangle\langle 1'_s| \sum_j \frac{1}{\omega_j} \left(\langle 1 | \hat{V}_j | 1 \rangle - s w_j^z \right) (\hat{b}_j^\dagger - \hat{b}_j) \right] \\ &= \sum_{s=\pm} |1'_s\rangle\langle 1'_s| \prod_j \hat{D}_j(\xi_j^s) \end{aligned} \quad (\text{S22})$$

where $\xi_j^s = (\langle 1|\hat{V}_j|1\rangle - sw_j^z) / \omega_j$ and

$$\hat{D}_j(\xi_j^s) = e^{\xi_j^s(\hat{b}_j^\dagger - \hat{b}_j)} \quad (\text{S23})$$

is the bosonic displacement operator acting on mode j , i.e. $\hat{D}_j(\xi)\hat{b}_j\hat{D}_j^\dagger(\xi) = \hat{b}_j - \xi$. The Hamiltonian thus becomes

$$\hat{S}\hat{H}_{\text{eff}}\hat{S}^\dagger = \sum_{s=\pm} |1'_s\rangle\langle 1'_s| \left(E_1 + s\frac{\Delta_1}{2} - \sum_j \omega_j |\xi_j^s|^2 \right) + \sum_j \omega_j \hat{b}_j^\dagger \hat{b}_j - \sum_j \hat{S} \left(w_j^x \sigma'_x + w_j^y \sigma'_y \right) \left(\hat{b}_j + \hat{b}_j^\dagger \right) \hat{S}^\dagger. \quad (\text{S24})$$

The polaron transformation reabsorbes the diagonal component of the spin-phonon coupling (S20) proportional to w_j^z into the energy shifts $\omega_j |\xi_j^\pm|^2$, leaving a residual off-diagonal spin-phonon coupling proportional to w_j^x and w_j^y . Note that the polaron transformation exactly diagonalises the Hamiltonian (S15) if $w_j^x = w_j^y = 0$. In Section S3, we argue in detail that in our case $|w_j^x|, |w_j^y| \ll |w_j^z|$ to a very good approximation. Based on this argument, we could decide to neglect the residual spin-phonon coupling in the polaron frame. The energies of the states belonging to the lowest doublet are shifted by a vibronic correction

$$E_{1'_\pm} = E_1 \pm \frac{\Delta_1}{2} - \sum_j \frac{1}{\omega_j} \left(\langle 1|\hat{V}_j|1\rangle \mp w_j^z \right)^2 \quad (\text{S25})$$

$$= E_1 \pm \frac{\Delta_1}{2} - \sum_j \frac{1}{\omega_j} \left(\langle 1|\hat{V}_j|1\rangle^2 \mp 2\langle 1|\hat{V}_j|1\rangle w_j^z + \mathcal{O}(B^2) \right), \quad (\text{S26})$$

leading to a redefinition of the energy gap

$$E_{1'_+} - E_{1'_-} = \Delta_1 + 4 \sum_j \frac{\langle 1|\hat{V}_j|1\rangle}{\omega_j} w_j^z. \quad (\text{S27})$$

Although the off-diagonal components of the spin-phonon coupling w_j^x and w_j^y are several orders of magnitude smaller than the diagonal one w_j^z (see Section S3), the sheer number of vibrational modes could still lead to an observable effect on the electronic degrees of freedom. We can estimate this effect by averaging the residual spin-phonon coupling over a thermal phonon distribution in the polaron frame. Making use of Eq. (S22), the off-diagonal coupling in Eq. (S24) can be written as

$$\begin{aligned} \hat{H}_{\text{sp-ph}}^{(\text{pol})} &= - \sum_j \hat{S} \left(w_j^x \sigma'_x + w_j^y \sigma'_y \right) \left(\hat{b}_j + \hat{b}_j^\dagger \right) \hat{S}^\dagger \\ &= - \sum_j |1'_-\rangle\langle 1_-|\hat{W}_j|1_+\rangle\langle 1'_+| \hat{D}_j(\xi_j^-) \left(\hat{b}_j + \hat{b}_j^\dagger \right) \hat{D}_j^\dagger(\xi_j^+) + \text{h.c.} \end{aligned} \quad (\text{S28})$$

Assuming the vibrations to be in a thermal state at temperature T in the polaron frame

$$\rho_{\text{ph}}^{(\text{th})} = \prod_j \rho_j^{(\text{th})} = \prod_j \frac{e^{-\omega_j \hat{b}_j^\dagger \hat{b}_j / k_B T}}{\text{Tr} \left[e^{-\omega_j \hat{b}_j^\dagger \hat{b}_j / k_B T} \right]}, \quad (\text{S29})$$

obtaining the average of Eq. (S28) reduces to calculating the dimensionless quantity

$$\begin{aligned} \kappa_j &= -\text{Tr} \left[\hat{D}_j(\xi_j^-) \left(\hat{b}_j + \hat{b}_j^\dagger \right) \hat{D}_j^\dagger(\xi_j^+) \rho_j^{(\text{th})} \right] \\ &= \left(\xi_j^+ + \xi_j^- \right) e^{-\frac{1}{2}(\xi_j^+ - \xi_j^-)^2 \coth\left(\frac{\omega_j}{2k_B T}\right)} \\ &= 2 \frac{\langle 1|\hat{V}_j|1\rangle}{\omega_j} e^{-2\frac{(w_j^z)^2}{\omega_j^2} \coth\left(\frac{\omega_j}{2k_B T}\right)} \\ &= 2 \frac{\langle 1|\hat{V}_j|1\rangle}{\omega_j} \left(1 + \mathcal{O}(B^2) \right), \end{aligned} \quad (\text{S30})$$

which appears as a multiplicative rescaling factor for the off-diagonal couplings $\langle 1_\mp|\hat{W}_j|1_\pm\rangle$. Note that, when neglecting second and higher order terms in the magnetic field, κ_j does not show any dependence on temperature or on the magnetic field orientation via θ_1 and ϕ_1 .

After thermal averaging, the effective electronic Hamiltonian for the lowest energy doublet becomes

$$\hat{H}_{\text{el}} = \text{Tr}_{\text{ph}} \left[\hat{S} \hat{H}_{\text{eff}} \hat{S}^\dagger \rho_{\text{ph}}^{(\text{th})} \right] = E_1 + \delta E_1 + \left(2 \sum_j \frac{\langle 1 | \hat{V}_j | 1 \rangle}{\omega_j} w_j^x, 2 \sum_j \frac{\langle 1 | \hat{V}_j | 1 \rangle}{\omega_j} w_j^y, \frac{\Delta_1}{2} + 2 \sum_j \frac{\langle 1 | \hat{V}_j | 1 \rangle}{\omega_j} w_j^z \right) \cdot \begin{pmatrix} \sigma'_x \\ \sigma'_y \\ \sigma'_z \end{pmatrix} \quad (\text{S31})$$

where the energy of the lowest doublet is shifted by

$$\delta E_1 = - \sum_j \frac{\langle 1 | \hat{V}_j | 1 \rangle^2}{\omega_j} + \sum_j \frac{\omega_j}{e^{\omega_j/k_B T} - 1} \quad (\text{S32})$$

due to the spin-phonon coupling and to the thermal phonon energy. Eq. (S31) thus represents a refined description of the lowest effective spin-1/2 doublet in the presence of spin-phonon coupling.

We can finally recast the Hamiltonian (S31) in terms of a g -matrix for an effective spin 1/2, similarly to what we did earlier in the case of no spin-phonon coupling. In order to do so, we first recall from Eq. (S11) and (S19) that the quantities Δ_1 and (w_j^x, w_j^y, w_j^z) appearing in Eq. (S31) depend on the magnetic field orientation via the states $|1_\pm\rangle$, and on both orientation and intensity via \hat{H}_{Zee} . We can get rid of the first dependence by expressing the Zeeman eigenstates $|1_\pm\rangle$ in terms of the original crystal field eigenstates $|1\rangle, |\bar{1}\rangle$. For the spin-phonon coupling vector \mathbf{w}_j , we obtain

$$\mathbf{w}_j = \begin{pmatrix} \Re \langle 1_- | \hat{W}_j | 1_+ \rangle \\ \Im \langle 1_- | \hat{W}_j | 1_+ \rangle \\ \langle 1_+ | \hat{W}_j | 1_+ \rangle \end{pmatrix} = \begin{pmatrix} \cos \theta_1 \cos \phi_1 & \cos \theta_1 \sin \phi_1 & -\sin \theta_1 \\ -\sin \phi_1 & \cos \phi_1 & 0 \\ \sin \theta_1 \cos \phi_1 & \sin \theta_1 \sin \phi_1 & \cos \theta_1 \end{pmatrix} \begin{pmatrix} \Re \langle \bar{1} | \hat{W}_j | 1 \rangle \\ \Im \langle \bar{1} | \hat{W}_j | 1 \rangle \\ \langle 1 | \hat{W}_j | 1 \rangle \end{pmatrix} = \mathbf{R}(\theta_1, \phi_1) \cdot \tilde{\mathbf{w}}_j. \quad (\text{S33})$$

where $\mathbf{R}(\theta_1, \phi_1)$ is a rotation matrix. Similarly, the electronic contribution Δ_1 transforms as

$$(0, 0, \Delta_1) = \mathbf{j}_1 \cdot \mathbf{R}(\theta_1, \phi_1)^T, = \mu_B \mathbf{B} \cdot \mathbf{g}_{\text{el}}^{(1)} \cdot \mathbf{R}(\theta_1, \phi_1)^T. \quad (\text{S34})$$

The Pauli spin operators need to be changed accordingly to $\tilde{\sigma} = \mathbf{R}(\theta_1, \phi_1)^T \cdot \sigma'$. Lastly, we single out explicitly the magnetic field dependence of \hat{W}_j , defined in Eq. (S18), by introducing a three-component operator $\hat{\mathbf{K}}_j = (\hat{K}_j^x, \hat{K}_j^y, \hat{K}_j^z)$, such that

$$\begin{aligned} \hat{W}_j &= \mu_B g_J \mathbf{B} \cdot (\hat{V}_j \hat{Q}_1 \hat{\mathbf{J}} + \hat{\mathbf{J}} \hat{Q}_1 \hat{V}_j) \\ &= \mu_B g_J \mathbf{B} \cdot \hat{\mathbf{K}}_j. \end{aligned} \quad (\text{S35})$$

Thus, the effective electronic Hamiltonian in Eq. (S31) can be finally rewritten as

$$\hat{H}_{\text{el}} = E_1 + \delta E_1 + \mu_B \mathbf{B} \cdot \left(\mathbf{g}_{\text{el}}^{(1)} + \mathbf{g}_{\text{vib}} \right) \cdot \tilde{\sigma} / 2 \quad (\text{S36})$$

where $\mathbf{g}_{\text{el}}^{(1)}$ is the electronic g -matrix defined in Eq. (S8), and

$$\mathbf{g}_{\text{vib}} = 4g_J \sum_j \frac{\langle 1 | \hat{V}_j | 1 \rangle}{\omega_j} \begin{pmatrix} \Re \langle \bar{1} | \hat{K}_j^x | 1 \rangle & \Im \langle \bar{1} | \hat{K}_j^x | 1 \rangle & \langle 1 | \hat{K}_j^x | 1 \rangle \\ \Re \langle \bar{1} | \hat{K}_j^y | 1 \rangle & \Im \langle \bar{1} | \hat{K}_j^y | 1 \rangle & \langle 1 | \hat{K}_j^y | 1 \rangle \\ \Re \langle \bar{1} | \hat{K}_j^z | 1 \rangle & \Im \langle \bar{1} | \hat{K}_j^z | 1 \rangle & \langle 1 | \hat{K}_j^z | 1 \rangle \end{pmatrix} \quad (\text{S37})$$

is a vibronic correction.

Note that this correction is non-perturbative in the spin-phonon coupling, despite only containing quadratic terms in \hat{V}_j (recall that $\hat{\mathbf{K}}_j$ depends linearly on \hat{V}_j). The only approximations leading to Eq. (S36) are a linear perturbative expansion in the magnetic field \mathbf{B} and neglecting quantum fluctuations of the off-diagonal spin-phonon coupling in the polaron frame, which is accounted for only via its thermal expectation value. This approximation relies on the fact that the off-diagonal couplings are much smaller than the diagonal spin-phonon coupling that is treated exactly by the polaron transformation (see Section S3).

C. Landau-Zener probability

Let us consider a situation in which the magnetic field comprises a time-independent contribution arising from internal dipolar or hyperfine fields \mathbf{B}_{int} and a time dependent external field $\mathbf{B}_{\text{ext}}(t)$. Let us fix the orientation of the external field and vary its magnitude at a constant rate, such that the field switches direction at $t = 0$. Under these circumstances, the Hamiltonian of Eq. (S36) becomes

$$\hat{H}_{\text{el}}(t) = E_1 + \delta E_1 + \mu_B \left(\mathbf{B}_{\text{int}} + \frac{d\mathbf{B}_{\text{ext}}}{dt} t \right) \cdot \mathbf{g} \cdot \frac{\tilde{\sigma}}{2}, \quad (\text{S38})$$

where $\mathbf{g} = \mathbf{g}_{\text{el}}^{(1)} + \mathbf{g}_{\text{vib}}$. Neglecting the constant energy shift and introducing the vectors

$$\mathbf{\Delta} = \mu_B \mathbf{B}_{\text{ext}} \cdot \mathbf{g}, \quad (\text{S39})$$

$$\mathbf{v} = \mu_B d\mathbf{B}_{\text{ext}}/dt \cdot \mathbf{g}, \quad (\text{S40})$$

the Hamiltonian then becomes

$$\hat{H}_{\text{el}}(t) = \frac{\mathbf{\Delta}}{2} \cdot \tilde{\boldsymbol{\sigma}} + \frac{\mathbf{v}t}{2} \cdot \tilde{\boldsymbol{\sigma}} = \frac{\mathbf{\Delta}_{\perp}}{2} \cdot \tilde{\boldsymbol{\sigma}} + \frac{\mathbf{v}t + \mathbf{\Delta}_{\parallel}}{2} \cdot \tilde{\boldsymbol{\sigma}}. \quad (\text{S41})$$

In the second equality, we have split the vector $\mathbf{\Delta} = \mathbf{\Delta}_{\perp} + \mathbf{\Delta}_{\parallel}$ into a perpendicular and a parallel component to \mathbf{v} . Choosing an appropriate reference frame, we can write

$$\hat{H}_{\text{el}}(t') = \frac{\Delta_{\perp}}{2} \tilde{\sigma}_x + \frac{vt'}{2} \tilde{\sigma}_z, \quad (\text{S42})$$

in terms of the new time variable $t' = t + \Delta_{\parallel}/v$. Assuming that the spin is initialised in its ground state at $t' \rightarrow -\infty$, the probability of observing a spin flip at $t' \rightarrow +\infty$ is given by the Landau-Zener formula [15–20]

$$P_{\text{LZ}} = 1 - \exp\left(-\frac{\pi \Delta_{\perp}^2}{2v}\right). \quad (\text{S43})$$

We remark that tunnelling is only made possible by the presence of Δ_{\perp} , which stems from internal fields that have a perpendicular component to the externally applied field. We also observe that a perfectly axial system would not exhibit tunnelling behaviour, since in that case the direction of $\mathbf{B} \cdot \mathbf{g}$ would always point along the easy axis (i.e. along the only eigenvector of \mathbf{g} with a non-vanishing eigenvalue), and therefore \mathbf{v} and $\mathbf{\Delta}$ would always be parallel. Thus, deviations from axially and the presence of transverse fields are both required for QTM to occur.

S3. DISTRIBUTION OF SPIN-PHONON COUPLING VECTORS

The effective polaron Hamiltonian presented in Eq. (7) and derived in the previous section provides a good description of the ground doublet only if the spin-phonon coupling operators are approximately diagonal in the electronic eigenbasis. This is equivalent to requiring that the components of the vectors \mathbf{w}_j defined in Eq. (S19) satisfy

$$|w_j^x|, |w_j^y| \ll |w_j^z|. \quad (\text{S44})$$

Fig. S1a shows the distribution of points $\{\mathbf{w}_j, j = 1, \dots, M\}$ (where M is the number of vibrational modes) in 3D space for different orientations of the magnetic field. As a consequence of the strong magnetic axially of the complex under consideration, we see that these points are mainly distributed along the z -axis, therefore satisfying the criterion expressed in Eq. (S44) (note the different scale on the xy -plane).

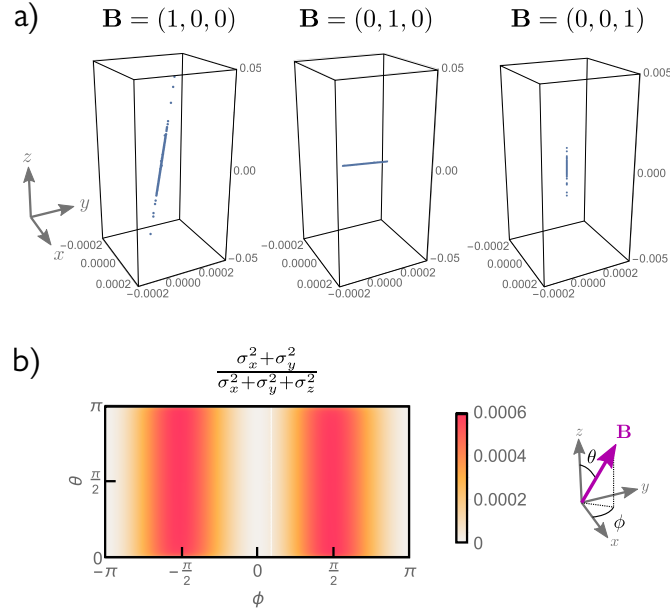


FIG. S1. **Distribution of spin-phonon coupling vectors \mathbf{w}_j .** (a) The points \mathbf{w}_j distribute along a straight line in 3D space (units: cm^{-1}) when the magnetic field is oriented along x , y , z . The magnitude is fixed to 1 T. Note that, owing to the definition of \mathbf{w}_j , a different magnitude would yield a uniformly rescaled distribution of points, leaving the shape unchanged. (b) Variance of the points \mathbf{w}_j in the xy -plane in units of the total variance, as a function of magnetic field orientation.

In order to confirm that the points \mathbf{w}_j maintain a similar distribution regardless of the magnetic field orientation, we calculate their variances along different directions of the 3D space they inhabit. We define

$$\sigma_\alpha^2 = \text{var}(w_j^\alpha) = \frac{1}{M-1} \sum_{j=1}^M (w_j^\alpha - \mu_\alpha)^2, \quad (\text{S45})$$

where $\alpha = x, y, z$ and $\mu_\alpha = \frac{1}{M} \sum_{j=1}^M w_j^\alpha$. The dependence of these variances on the field orientation is made evident by recalling that the points \mathbf{w}_j are related via a rotation $\mathbf{R}(\theta_1, \phi_1)$ to the set of points $\tilde{\mathbf{w}}_j$, which only depend linearly on the field \mathbf{B} , as shown in Eqs. (S33) and (S35). If the points are mainly distributed along z for any field orientation, we expect the combined variance in the xy -plane to be much smaller than the total variance of the dataset, i.e.

$$\sigma_x^2 + \sigma_y^2 \ll \sigma_x^2 + \sigma_y^2 + \sigma_z^2. \quad (\text{S46})$$

Fig. S1b provides a direct confirmation of this hypothesis, showing that the variance in the xy -plane is at most 6×10^{-4} times smaller than the total variance. Therefore, we conclude that the approach followed in Section S2 is fully justified.

S4. EXPERIMENTAL ESTIMATE OF THE SPIN-FLIP PROBABILITY

In order to provide experimental support for our vibronic model of QTM, we compare the calculated spin-flip probabilities with values extracted from previously reported measurements of magnetic hysteresis. We use data from field-dependent magnetisation measurements reported in Ref. [7](Fig. S35, sample 4), reproduced here in Fig. S2. The sample consisted of a 83 μL volume of a 170 mM solution of $[\text{Dy}(\text{Cp}^{\text{III}})_2][\text{B}(\text{C}_6\text{F}_5)_4]$ in dichloromethane (DCM). The field-dependent magnetisation was measured at $T = 2$ K while sweeping an external magnetic field B_{ext} from +7 T to -7 T and back again to +7 T. The resulting hysteresis loop is shown in Fig. S2a. The sweep rate dB_{ext}/dt is not constant throughout the hysteresis loop, as shown in Fig. S2b. In particular, it takes values between 10 Oe/s and 20 Oe/s across the zero field region where QTM takes place.

QTM results in a characteristic step around the zero field region in magnetic hysteresis curves (Fig. S2a). The spin-flip probability across the tunnelling transition can be easily related to the height of this step via the expression [21]

$$P_{\uparrow \rightarrow \downarrow} = \frac{1}{2} \left(\frac{M}{M_{\text{sat}}} - \frac{M'}{M_{\text{sat}}} \right). \quad (\text{S47})$$

The value of the magnetisation before (M) and after (M') the QTM drop is estimated by performing a linear fit of the field-dependent magnetisation close to the zero field region, for both $B_{\text{ext}} > 0$ and $B_{\text{ext}} < 0$, and extrapolating the magnetisation at $B_{\text{ext}} = 0$ (Fig. S2a, inset). The saturation value of the magnetisation M_{sat} is obtained by measuring the magnetisation at low temperature in a strong external magnetic field ($T = 2$ K, $B_{\text{ext}} = 7$ T). Following this method, we obtain a spin-flip probability $P_{\uparrow \rightarrow \downarrow} = 0.27$, which is shown as a purple horizontal line in Fig. 4 in the main text.

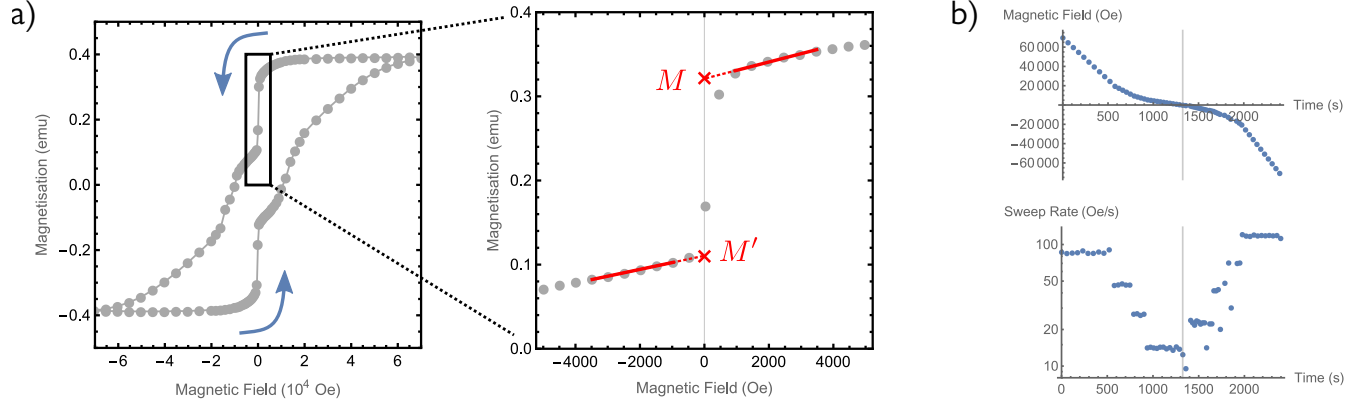


FIG. S2. **Magnetic hysteresis of $[\text{Dy}(\text{Cp}^{\text{III}})_2]^+$ from Ref. [7].** (a) Field-dependent magnetisation was measured on a 170 mM frozen solution of $[\text{Dy}(\text{Cp}^{\text{III}})_2]^+$ (counter ion $[\text{B}(\text{C}_6\text{F}_5)_4]^-$) in DCM at $T = 2$ K. Data presented in [7] (Fig. S35, sample 4). The loop is traversed in the direction indicated by the blue arrows. The sudden drop of the magnetisation from M to M' around $B_{\text{ext}} = 0$ is a characteristic signature of QTM. The slow magnetisation decay around the QTM step can be ascribed to other magnetic relaxation mechanisms (Raman). (b) Time dependence of the magnetic field B_{ext} (top) and instantaneous sweep rate (bottom). Note that the sweep rate is not constant around the avoided crossing at $B_{\text{ext}} = 0$, but assumes values in the range 10–20 Oe/s.

S5. ESTIMATE OF THE INTERNAL FIELDS IN A FROZEN SOLUTION

A. Dipolar fields

In this section we provide an estimate of the internal fields B_{int} in a disordered ensemble of SMMs, based on field-dependent magnetisation data introduced in Section S4.

When a SMM with strongly axial magnetic anisotropy is placed in a strong external magnetic field \mathbf{B}_{ext} , it gains a non-zero magnetic dipole moment along its easy axis. Once the external field is removed, the SMM partially retains its magnetisation $\boldsymbol{\mu} = \mu \hat{\boldsymbol{\mu}}$, which produces a microscopic dipolar field

$$\mathbf{B}_{\text{dip}}(\mathbf{r}) = \frac{\mu_0 \mu}{4\pi r^3} [3\hat{\mathbf{r}}(\hat{\boldsymbol{\mu}} \cdot \hat{\mathbf{r}}) - \hat{\boldsymbol{\mu}}] \quad (\text{S48})$$

at a point $\mathbf{r} = r\hat{\mathbf{r}}$ in space. This field can then cause a tunnelling gap to open in neighboring SMMs, depending on their relative distance and orientation.

In order to estimate the strength of typical dipolar fields, we need to determine the average distance between SMMs in the sample, and the magnetic dipole moment associated with a single SMM. Since we know both volume V and concentration of Dy centres in the sample (see previous section), we can easily obtain the number of SMMs in solution N . The average distance between SMMs can then be obtained simply by taking the cubic root of the volume per particle, as

$$r = \left(\frac{V}{N}\right)^{1/3} \approx 21.4 \text{ \AA}. \quad (\text{S49})$$

The magnetic moment can be obtained from the hysteresis curve shown in Fig. S2a, by reading the value of the magnetisation M right before the QTM step. This amounts to an average magnetic moment per molecule

$$\langle \mu_{\parallel} \rangle = \frac{M}{N} \approx 4.07 \mu_{\text{B}}, \quad (\text{S50})$$

along the direction of the external field \mathbf{B}_{ext} , where $\langle \cdot \rangle$ denotes the average over the ensemble of SMMs. Since the orientation of SMMs in a frozen solution is random, the component of the magnetisation $\boldsymbol{\mu}$ perpendicular to the applied field averages to zero, i.e. $\langle \mu_{\perp} \rangle = 0$. However, it still contributes to the formation of the microscopic dipolar field (S48), which depends on $\boldsymbol{\mu} = \mu_{\parallel} + \mu_{\perp}$. Since the sample consists of many randomly oriented SMMs, the average magnetisation in Eq. (S50) can also be expressed in terms of $\mu = |\boldsymbol{\mu}|$ via the orientational average

$$\langle \mu_{\parallel} \rangle = \int_0^{\pi/2} d\theta \sin \theta \mu_{\parallel}(\theta) = \frac{\mu}{2}, \quad (\text{S51})$$

where $\mu_{\parallel}(\theta) = \mu \cos \theta$ is the component of the magnetisation of a SMM along the direction of the external field \mathbf{B}_{ext} . Thus, the magnetic moment responsible for the microscopic dipolar field is twice as big as the measured value (S50).

Based on these estimates, the magnitude of dipolar fields experienced by a Dy atom in the sample is

$$B_{\text{dip}} = 0.77 \text{ mT} \times \sqrt{|3(\hat{\boldsymbol{\mu}} \cdot \hat{\mathbf{r}})^2 - 1|}. \quad (\text{S52})$$

The square root averages to 1.38 for randomly oriented $\boldsymbol{\mu}$ and \mathbf{r} and can take values between 1 and 2, represented by the green shaded area in Fig. 4 in the main text.

B. Hyperfine coupling

Another possible source of microscopic magnetic fields are nuclear spins. Among the different isotopes of dysprosium, only ^{161}Dy and ^{163}Dy have non-zero nuclear spin ($I = 5/2$), making up for approximately 44 % of naturally occurring dysprosium.

The nuclear spin degrees of freedom are described by the Hamiltonian

$$\hat{H}_{\text{nuc}} = \hat{H}_{\text{Q}} + \hat{H}_{\text{HF}} = \hat{\mathbf{I}} \cdot \mathbf{P} \cdot \hat{\mathbf{I}} + \hat{\mathbf{I}} \cdot \mathbf{A} \cdot \hat{\mathbf{J}}, \quad (\text{S53})$$

where the first term is the quadrupole Hamiltonian $\hat{H}_{\text{Q}} = \hat{\mathbf{I}} \cdot \mathbf{P} \cdot \hat{\mathbf{I}}$, accounting for the zero-field splitting of the nuclear spin states, and the second term $\hat{H}_{\text{HF}} = \hat{\mathbf{I}} \cdot \mathbf{A} \cdot \hat{\mathbf{J}}$ accounts for the hyperfine coupling between nuclear spin $\hat{\mathbf{I}}$ and electronic angular momentum

$\hat{\mathbf{J}}$ operators. In analogy with the electronic Zeeman Hamiltonian $\hat{H}_{Zee} = \mu_B g_J \mathbf{B} \cdot \hat{\mathbf{J}}$, we define the effective nuclear magnetic field operator

$$\mu_B g_J \hat{\mathbf{B}}_{\text{nuc}} = \mathbf{A}^T \cdot \hat{\mathbf{I}}, \quad (\text{S54})$$

so that the hyperfine coupling Hamiltonian takes the form of a Zeeman interaction $\hat{H}_{\text{HF}} = \mu_B g_J \hat{\mathbf{B}}_{\text{nuc}}^\dagger \cdot \hat{\mathbf{J}}$. If we consider the nuclear spin to be in a thermal state at temperature T with respect to the quadrupole Hamiltonian \hat{H}_Q , the resulting expectation value of the nuclear magnetic field vanishes, since the nuclear spin is completely unpolarised. However, the external field \mathbf{B}_{ext} will tend to polarise the nuclear spin via the nuclear Zeeman Hamiltonian

$$\hat{H}_{\text{nuc, Zee}} = \mu_N g \mathbf{B}_{\text{ext}} \cdot \hat{\mathbf{I}}, \quad (\text{S55})$$

where μ_N is the nuclear magneton and g is the nuclear g -factor of a Dy nucleus. In this case, the nuclear spin is described by the thermal state

$$\rho_{\text{nuc}}^{(\text{th})} = \frac{e^{-(\hat{H}_Q + \hat{H}_{\text{nuc, Zee}})/k_B T}}{\text{Tr} \left[e^{-(\hat{H}_Q + \hat{H}_{\text{nuc, Zee}})/k_B T} \right]} \quad (\text{S56})$$

and the effective nuclear magnetic field can be calculated as

$$\mathbf{B}_{\text{nuc}} = \text{Tr} \left[\hat{\mathbf{B}}_{\text{nuc}} \rho_{\text{nuc}}^{(\text{th})} \right]. \quad (\text{S57})$$

To the best of our knowledge, quadrupole and hyperfine coupling tensors for Dy in $[\text{Dy}(\text{Cp}^{\text{ttt}})_2]^+$ have not been reported in the literature. However, *ab initio* calculations of hyperfine coupling tensors have been performed on DyPc₂ [22]. Although the dysprosium atom in DyPc₂ and $[\text{Dy}(\text{Cp}^{\text{ttt}})_2]^+$ interacts with different ligands, the crystal field is qualitatively similar for these two complexes, therefore we expect the nuclear spin Hamiltonian to be sufficiently close to the one for $[\text{Dy}(\text{Cp}^{\text{ttt}})_2]^+$, at least for the purpose of obtaining an approximate estimate. Using the quadrupolar and hyperfine tensors determined for DyPc₂ [22] and the nuclear g -factors measured for ¹⁶¹Dy and ¹⁶³Dy [23], we can compute $B_{\text{nuc}} = |\mathbf{B}_{\text{nuc}}|$ from Eq. (S57) for different orientations of the external magnetic field. As shown in Table S1, the effective nuclear magnetic fields at $T = 2$ K are at least one order of magnitude smaller than the dipolar fields calculated in the previous section, regardless of the orientation of the external field.

	¹⁶¹ Dy	¹⁶³ Dy
$\mathbf{B}_{\text{ext}}/\hat{\mathbf{x}}$	2.82×10^{-8}	5.34×10^{-8}
$\mathbf{B}_{\text{ext}}/\hat{\mathbf{y}}$	1.77×10^{-8}	3.38×10^{-8}
$\mathbf{B}_{\text{ext}}/\hat{\mathbf{z}}$	5.51×10^{-5}	1.08×10^{-4}

TABLE S1. Effective Dy nuclear magnetic field B_{nuc} (T) at $T = 2$ K.

S6. RESULTS FOR A DIFFERENT SOLVENT CONFIGURATION

In this section we show that the results presented in the main text are robust against variations of the solvent environment on a qualitative level. In order to show this, we consider a smaller and rounder solvent ball consisting of 111 DCM molecules, and reproduce the results shown in the main text, as shown in Fig. S3. It is worth noting that the vibronic spin-flip probabilities are significantly smaller for the smaller solvent ball, confirming the importance of the low-frequency vibrational modes associated to the solvent for determining QTM behaviour. The general tendency of vibrations to enhance QTM, however, is correctly reproduced.

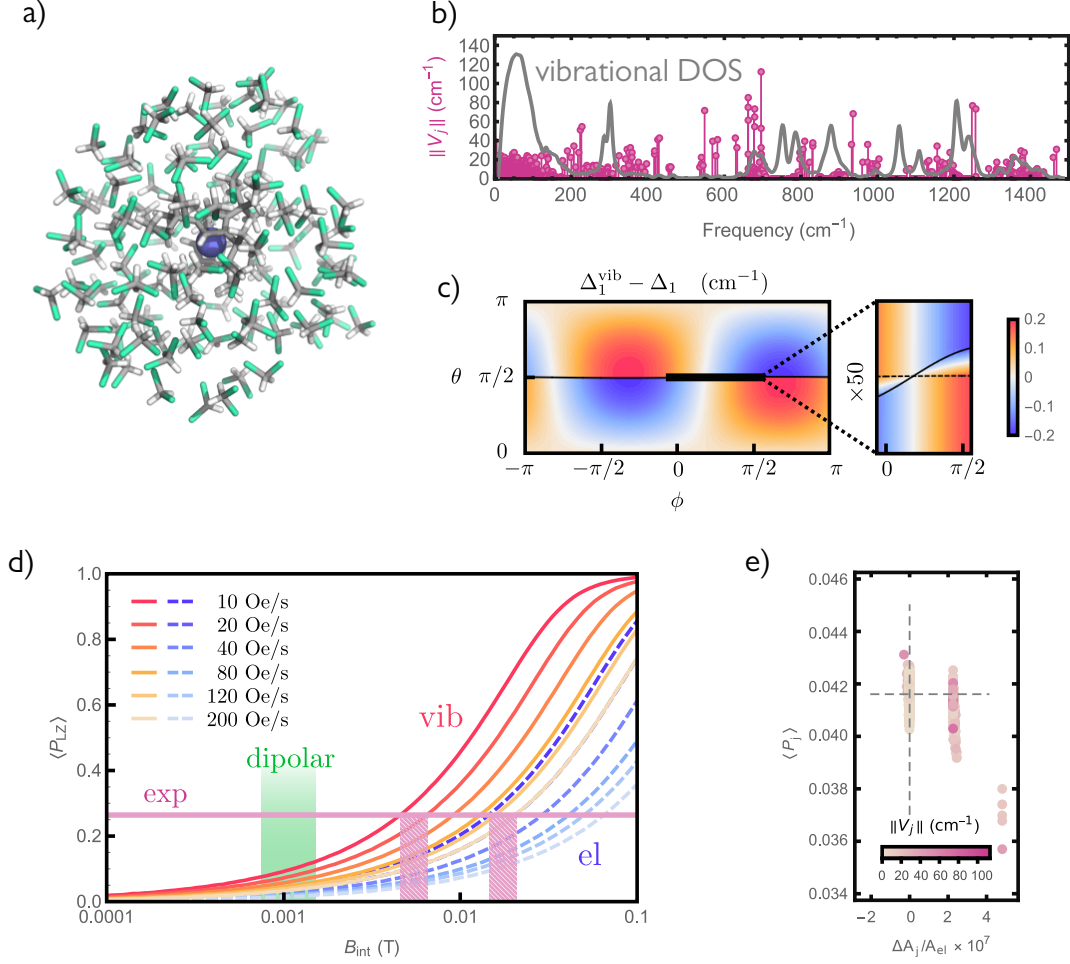


FIG. S3. **Results for a different solvent configuration.** (a) Alternative arrangement of 111 DCM molecules around $[\text{Dy}(\text{Cp}^{\text{III}})_2]^+$. (b) Spin-phonon coupling strength and vibrational density of states (see Fig. 1c). (c) Vibronic correction to the energy splitting of the ground Kramers doublet ($\Delta_1^{\text{vib}} - \Delta_1$) for different orientations of the magnetic field (see Fig. 2a). (d) Ensemble-averaged spin-flip probability for different field sweep rates as a function of the internal field strength (see Fig. 3). (e) Orientationally averaged single-mode spin-flip probability $\langle P_j \rangle$ vs change in magnetic axiality $\Delta A_j/A_{\text{el}}$ (see Fig. 4).

The most evident difference between these results and the ones presented in the main text is the shape of the single-mode axiality distribution (Fig. S3e). In this case, single-mode spin-flip probability $\langle P_j \rangle$ still correlates to relative single-mode axiality $\Delta A_j/A_{\text{el}}$. However, instead of taking values on a continuous range, the relative axiality seems to cluster around discrete values. In an attempt to clarify the origin of this strange behaviour, we looked at the composition of the vibrational modes belonging to the different clusters. Vibrational modes belonging to the same cluster were not found to share any evident common feature. Rather than in the structure of the vibrational modes, this behaviour seems to originate from the equilibrium electronic g -matrix g^{el} . This can be seen by computing the single-mode axiality $A_j = A(g^{\text{el}} + \mathbf{g}_j^{\text{vib}})$ for slightly different choices of g^{el} . In particular, we checked how axiality of the electronic g -matrix affects the mode axiality. In order to do that, we considered the singular value decomposition of the electronic g -matrix

$$g^{\text{el}} = \mathbf{U} \cdot \text{diag}(g_1, g_2, g_3) \cdot \mathbf{V}^\dagger, \quad (\text{S58})$$

the matrices \mathbf{U} and \mathbf{V} contain its left and right eigenvectors. The singular values are $g_1 = 19.99$, $g_2 = 3.40 \times 10^{-6}$, $g_3 = 2.98 \times 10^{-6}$, and the axiality is very close to one, i.e. $1 - A_{\text{el}} = 4.79 \times 10^{-7}$. We artificially change the axiality of \mathbf{g}^{el} by rescaling the hard-plane g -values by a factor α and redefining the electronic g -matrix as

$$g_{\alpha}^{\text{el}} = \mathbf{U} \cdot \text{diag}(g_1, \alpha g_2, \alpha g_3) \cdot \mathbf{V}^{\dagger}. \quad (\text{S59})$$

The results are shown in Fig. S4. The three different colours distinguish the vibrational modes belonging to the three clusters visible in Fig. S3e (corresponding to $\alpha = 1$). When $\alpha = 0$, the g -matrix has perfect easy-axis anisotropy. In this case, the vibronic correction to the g -matrix is too small to cause significant changes in the magnetic axiality, and all the vibrational modes align around $A_j \approx A_{\text{el}}$. Increasing α to 0.9, clusters begin to appear. For $\alpha = 1.3$, the single-mode axiality distribution begins to look like the one shown in Fig. 4a in the main text. The electronic g -matrix obtained for the solvent ball considered in the main text has a lower axiality than the one used throughout this section, i.e. $1 - A_{\text{el}} = 1.12 \times 10^{-6}$. Therefore, it makes sense that for α sufficiently larger than 1 we recover the same type of distribution as in the main text, since increasing α corresponds to lowering the electronic axiality $A(\mathbf{g}_{\alpha}^{\text{el}})$.

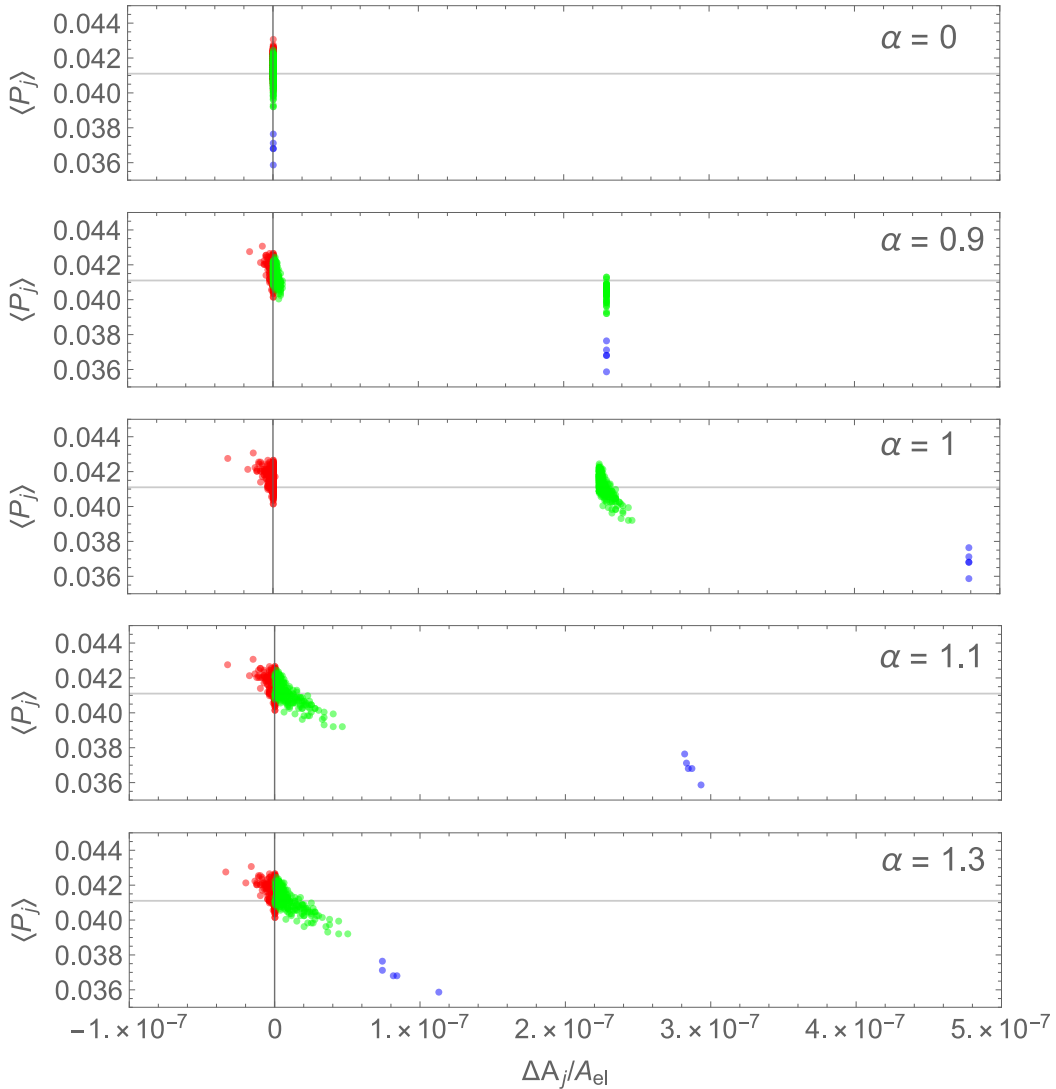


FIG. S4. **Impact of electronic axiality on single-mode axiality.** Distribution of single-mode spin-flip probability $\langle P_j \rangle$ and g -matrix axiality $A_j = A(\mathbf{g}_{\alpha}^{\text{el}} + \mathbf{g}_j^{\text{vib}})$ relative to the axiality of the modified electronic g -matrix $A(\mathbf{g}_{\alpha}^{\text{el}})$ defined in Eq. (S59). Vibrational modes belonging to different clusters in Fig. S3e ($\alpha = 1$) are labelled with different colors.

-
- [1] M. Svensson, S. Humbel, R. D. J. Froese, T. Matsubara, S. Sieber, and K. Morokuma, *ONIOM: a multilayered integrated MO + MM method for geometry optimizations and single point energy predictions. a test for diels-alder reactions and Pt(P(t-Bu)₃)₂ + H₂ oxidative addition*, The Journal of Physical Chemistry **100**, 19357 (1996).
- [2] J. P. Perdew, K. Burke, and M. Ernzerhof, *Generalized gradient approximation made simple*, Physical Review Letters **77**, 3865 (1996).
- [3] D. Andrae, U. Häußermann, M. Dolg, H. Stoll, and H. Preuß, *Energy-adjusted ab initio pseudopotentials for the second and third row transition elements*, Theor. Chim. Acta **77**, 123 (1990).
- [4] T. H. Dunning, *Gaussian basis sets for use in correlated molecular calculations. i. the atoms boron through neon and hydrogen*, The Journal of Chemical Physics **90**, 1007 (1989).
- [5] M. J. Frisch, G. W. Trucks, H. B. Schlegel, G. E. Scuseria, M. A. Robb, J. R. Cheeseman, G. Scalmani, V. Barone, B. Mennucci, G. A. Petersson, H. Nakatsuji, M. Caricato, X. Li, H. P. Hratchian, A. F. Izmaylov, J. Bloino, G. Zheng, J. L. Sonnenberg, M. Hada, M. Ehara, K. Toyota, R. Fukuda, J. Hasegawa, M. Ishida, T. Nakajima, Y. Honda, O. Kitao, H. Nakai, T. Vreven, J. A. Montgomery, Jr., J. E. Peralta, F. Ogliaro, M. Bearpark, J. J. Heyd, E. Brothers, K. N. Kudin, V. N. Staroverov, R. Kobayashi, J. Normand, K. Raghavachari, A. Rendell, J. C. Burant, S. S. Iyengar, J. Tomasi, M. Cossi, N. Rega, J. M. Millam, M. Klene, J. E. Knox, J. B. Cross, V. Bakken, C. Adamo, J. Jaramillo, R. Gomperts, R. E. Stratmann, O. Yazyev, A. J. Austin, R. Cammi, C. Pomelli, J. W. Ochterski, R. L. Martin, K. Morokuma, V. G. Zakrzewski, G. A. Voth, P. Salvador, J. J. Dannenberg, S. Dapprich, A. D. Daniels, O. Farkas, J. B. Foresman, J. V. Ortiz, J. Cioslowski, and D. J. Fox, Gaussian 09 Revision D.01, (2009), Gaussian Inc. Wallingford CT.
- [6] I. Fdez. Galván, M. Vacher, A. Alavi, C. Angeli, F. Aquilante, J. Autschbach, J. J. Bao, S. I. Bokarev, N. A. Bogdanov, R. K. Carlson, L. F. Chibotaru, J. Creutzberg, N. Dattani, M. G. Delcey, S. S. Dong, A. Dreuw, L. Freitag, L. M. Frutos, L. Gagliardi, F. Gendron, A. Giussani, L. González, G. Grell, M. Guo, C. E. Hoyer, M. Johansson, S. Keller, S. Knecht, G. Kovačević, E. Källman, G. Li Manni, M. Lundberg, Y. Ma, S. Mai, J. P. Malhado, P. Å. Malmqvist, P. Marquetand, S. A. Mewes, J. Norell, M. Olivucci, M. Oppel, Q. M. Phung, K. Pierloot, F. Plasser, M. Reiher, A. M. Sand, I. Schapiro, P. Sharma, C. J. Stein, L. K. Sørensen, D. G. Truhlar, M. Ugandi, L. Ungur, A. Valentini, S. Vancoillie, V. Velyazov, O. Weser, T. A. Wesolowski, P.-O. Widmark, S. Wouters, A. Zech, J. P. Zobel, and R. Lindh, *Openmolcas: From source code to insight*, Journal of Chemical Theory and Computation **15**, 5925 (2019).
- [7] C. A. P. Goodwin, F. Ortu, D. Reta, N. F. Chilton, and D. P. Mills, *Molecular magnetic hysteresis at 60 kelvin in dysprosocenium*, Nature **548**, 439 (2017).
- [8] C. M. Breneman and K. B. Wiberg, *Determining atom-centered monopoles from molecular electrostatic potentials. the need for high sampling density in formamide conformational analysis*, Journal of Computational Chemistry **11**, 361 (1990).
- [9] P.-Å. Malmqvist and B. O. Roos, *The CASSCF state interaction method*, Chemical Physics Letters **155**, 189 (1989).
- [10] P.-Å. Malmqvist, B. O. Roos, and B. Schimmelpfennig, *The restricted active space (RAS) state interaction approach with spin-orbit coupling*, Chemical Physics Letters **357**, 230 (2002).
- [11] P.-O. Widmark, P.-Å. Malmqvist, and B. O. Roos, *Density matrix averaged atomic natural orbital (ANO) basis sets for correlated molecular wave functions*, Theoretica Chimica Acta **77**, 291 (1990).
- [12] F. Aquilante, R. Lindh, and T. B. Pedersen, *Unbiased auxiliary basis sets for accurate two-electron integral approximations*, The Journal of Chemical Physics **127**, 114107 (2007).
- [13] J. K. Staab and N. F. Chilton, *Analytic linear vibronic coupling method for first-principles spin-dynamics calculations in single-molecule magnets*, Journal of Chemical Theory and Computation (2022), 10.1021/acs.jctc.2c00611.
- [14] L. F. Chibotaru, A. Ceulemans, and H. Bolvin, *Unique definition of the Zeeman-splitting g tensor of a Kramers doublet*, Phys. Rev. Lett. **101**, 033003 (2008).
- [15] L. D. Landau, *Zur Theorie der Energieübertragung*, Phys. Z. Sowjetunion **1**, 88 (1932).
- [16] L. D. Landau, *Zur Theorie der Energieübertragung II*, Phys. Z. Sowjetunion **2**, 46 (1932).
- [17] C. Zener and R. H. Fowler, *Non-adiabatic crossing of energy levels*, Proceedings of the Royal Society of London. Series A **137**, 696 (1932).
- [18] E. C. G. Stückelberg, *Theorie der unelastischen Stöße zwischen Atomen*, Helv. Phys. Acta **5**, 369 (1932).
- [19] E. Majorana, *Atomi orientati in campo magnetico variabile*, Il Nuovo Cimento **9**, 43 (1932).
- [20] O. V. Ivakhnenko, S. N. Shevchenko, and F. Nori, *Nonadiabatic Landau-Zener-Stückelberg-Majorana transitions, dynamics, and interference*, Physics Reports **995**, 1 (2023).
- [21] G. Taran, E. Bonet, and W. Wernsdorfer, *Decoherence measurements in crystals of molecular magnets*, Phys. Rev. B **99**, 180408 (2019).
- [22] A. L. Wysocki and K. Park, *Hyperfine and quadrupole interactions for Dy isotopes in DyPc₂ molecules*, Journal of Physics: Condensed Matter **32**, 274002 (2020).
- [23] J. Ferch, W. Dankwort, and H. Gebauer, *Hyperfine structure investigations in DyI with the atomic beam magnetic resonance method*, Physics Letters A **49**, 287 (1974).